The copyright of this thesis vests in the author. No quotation from it or information derived from it is to be published without full acknowledgement of the source. The thesis is to be used for private study or non-commercial research purposes only.

Published by the University of Cape Town (UCT) in terms of the non-exclusive license granted to UCT by the author.

University of Cape Town

Silicon nanoparticle synthesis through thermal catalytic pyrolysis

University of Cape Town

A dissertation submitted to the Department of Physics, Faculty of Science at the University of Cape Town in fulfilment of the requirements for the degree of
Master of Science.

Manfred R. Scriba
28 September 2006

Supervised by: Prof M. Härting and Prof. D.T. Britton

University of Cape Town

ABSTRACT

Nanoparticles are considered as fundamental building blocks of nanotechnology and, silicon nanoparticles in particular, will form the basis of applications in single electron transistors, floating gate memory devices, solid state lighting, chemical sensors and flexible electronics, including solar cells and luminescent materials, printed on paper.

A remaining key challenge however in the development of applications is the reproducible and reliable production of nanomaterial in sufficient quantities. Historically nanoparticles have been manufactured by top-down approaches such as milling, laser ablation or etching, and bottom-up synthesis such as colloidal chemistry and gas phase pyrolysis. The chemical processes in the latter are generally equivalent to those in the chemical vapour deposition (CVD) of compact films. Due to its simplicity and the relatively straight-forward construction of the hot wire chemical vapour deposition (HWCVD) reactor, this method is further investigated as a suitable route to nanoparticle production.

The objective of this research is thus to produce Si nanoparticles (powder) in sufficient quantities, through thermal catalytic pyrolysis, while maintaining control of the important properties namely size, size distribution, composition and crystallinity.

Learning from HWCVD production parameters, a system was designed and constructed, mostly from used parts, which incorporates a water-cooled carousel that allows 6 depositions without compromising the vacuum. Si nanoparticles were produced with silane as precursor and hydrogen dilutions ranging from 0 to 80% and at operating pressures of 3 to 48 mbar. The material was characterised for morphology, bonding configuration and crystallinity using scanning electron microscopy (SEM), energy dispersive x-ray spectroscopy (EDX), Fourier transform infrared spectroscopy (FTIR), X-ray diffraction (XRD) and Raman spectroscopy respectively.

University of Cape Town

EDX and FTIR spectra of the particles reveal high concentrations of oxygen in all samples, and FTIR spectra indicate the presence of surface bound hydrogen. The material can thus be classified as hydrogenated amorphous silicon nanoparticles (a-Si:H) with substantial surface oxidisation. XRD and Raman spectra indicate a small fraction of crystalline order in samples produced at temperatures exceeding 120 °C. The research has successfully demonstrated that thermal catalytic pyrolysis can produce a-Si:H nanoparticles. The particles are mostly amorphous, hydrogenated and surface oxidised.

University of Cape Town

CONTENTS

ABSTRACT i
CONTENTS iii
1. INTRODUCTION 1
2. OVERVIEW OF NANOPARTICLE PRODUCTION METHODS 5
  2.1 'Top-down' production 6
  2.2 'Bottom-up' production 8
3. HOT WIRE CHEMICAL VAPOUR DEPOSITION 12
  3.1 The HWCVD process 13
  3.2 HWCVD for nanoparticle synthesis 16
4. THERMAL CATALYTIC PYROLYSIS SYSTEM 18
  4.1 System overview 19
  4.2 Reaction chamber 21
  4.3 Vacuum pump and gas handling 26
  4.4 Filament and power supply 27
  4.5 System performance 29
5. SILICON NANOPARTICLE PRODUCTION AND CHARACTERISATION 37
  5.1 Powder production 39
  5.2 Characterisation techniques 43
6. RESULTS AND DISCUSSION 52
  6.1 General appearance and yield of the Si produced 52
  6.2 Microstructure and morphology 54
  6.3 Particle composition 61
  6.4 Crystallinity and crystalline fraction 66
7. CONCLUSION 70
REFERENCES 72
APPENDIX "A": Gas handling safety control-sheet 78
APPENDX "B": Gas safety posters 79

University of Cape Town

University of Cape Town

1. INTRODUCTION

Nanoscience and Nanotechnology is an emerging field of science. Nanoscience is concerned with the understanding, prediction and control of novel and fundamental properties of materials arising from their nano-scale. Nanotechnology can be understood as the application and exploitation of these novel properties. At present, it is generally accepted that, for a particle or structure to qualify as nanostructured, at least one dimension should be in the order of, or smaller than 100 nm. Nanotechnology has, so far, found application in fields as diverse as textiles, cosmetics, drug delivery, diagnostics, catalysis, displays, batteries, solar and fuel cells. Other applications in development [1] are based on the success in the synthesis and properties of nano-particles and nano-structures.

In an attempt to clarify nanostructured materials three categories have been suggested [2]. The first category comprises nano-sized particles, wires or thin films that may be isolated or substrate supported. The second category comprises materials and devices in which the nanometre-size microstructure is limited to a thin surface region of the bulk material i.e. due to chemical and/or atomic modification of the surface on nanometre scale. The third category comprises bulk solids with nanometre-scale microstructures i.e. bulk solids in which the chemical composition, atomic arrangement and/or the size of the building blocks (e.g. crystallites, particles or molecular groups) forming the solid, vary on a length scale of a few nanometres throughout the bulk.

The challenge for the development of applications is the reproducible and reliable production of nanomaterial in sufficient quantities. As with all nanoscale systems there are two approaches: top-down and bottom-up [1]. In the case of nanoparticles a top-down approach to their production means a size reduction of the same bulk material. A bottom-up approach describes the synthesis of nanoparticles from chemically different precursors. Using these definitions, a top-down production includes all mechanical milling and chemical etching methods, as well as evaporation and condensation of the bulk material using, e.g. laser ablation. Bottom-up synthesis includes soft chemical

University of Cape Town

synthesis, or colloidal chemistry approaches as well as gas phase synthesis methods such as pyrolysis of a precursor gas.

The research presented in this thesis is primarily concerned with the synthesis of nanoparticles, specifically silicon nanoparticles.

In general, due to their small size, nanoparticles have a large surface to volume ratio, typically having a specific surface area of 400 $m^2.g^{-1}$ or higher [3], resulting in the domination of the surface properties of the particles. The chemical, electronic, optical, magnetic and mechanical properties of the nanoparticles become distinctively different from their bulk material. For instance [4], the following properties are all surface dependant, and as the particle size is decreased: the catalytic activity increases; mechanical reinforcement in nanocomposites increases, e.g. carbon black in rubber; electrical conductivity of ceramics increases; but electrical conductivity of metals decreases; the hardness and strength of metals increases; the ductility, hardness and formability of ceramics increases; but the sintering and super-plastic forming temperature of ceramic e.g. TiO_2 decreases; and the luminescence of semiconductors such as Si, GaAs, $ZnS:Mn^{+2}$ increases.

When nanoparticles are smaller than about 20 nm the electrons are confined to a very small domain and will start adopting energy levels which are determined by quantum "confinement" effects. Such particles are usually semiconducting e.g. Si, CdSe and CdS, and are known as quantum dots. The particle is said to behave like a large atom and is often called an "artificial atom" [5]. Quantum confinement leads to unexpected effects e.g. the modification of the optoelectronic properties as compared to that of the bulk material. Another advantage of semiconductor quantum dots stems from the very long life time of electrons in the excited states, which is an important requirement in laser optical applications [6].

The size effects described above also apply to silicon. Silicon quantum dots can be used to produce light emitters of various colours by "band-gap tuning", using particle size effects rather than the current complex techniques of synthesizing compound

University of Cape Town

semiconductors [5]. Silicon nanocrystals are also of interest for applications in solid state lighting. While bulk silicon shows basically no photoluminescence due to its indirect band-gap, strong photoluminescence has been demonstrated for silicon nanocrystals, even at room temperature [6]. The size-tuneable optical and electronic properties of silicon nanoparticles make silicon nanocrystals interesting candidates for a wide spectrum of high end applications, including light emitting diodes (LEDs), quantum dot lasers, chemical sensors and molecular electronics. Further low end applications include printed electronics and flexible solar cells [7] as well as luminescent materials and composites [5]. These applications are expected to benefit social as well as industrial use. Silicon nanoparticles are furthermore widely considered as a material with great potential for a wide spectrum of electronic applications and novel devices. A variety of novel electronic devices such as single electron transistors, vertical transistors and floating gate memory devices have been demonstrated. Furthermore, Si nanoparticle floating-gate memories have the potential to outperform conventional devices with faster read and write times, higher reliability, and lower power dissipation [8]. However, if these applications are to be commercially viable, these particles have to be produced in considerable quantities. A number of routes to the synthesis of silicon and other nanoparticles will be investigated and discussed in this thesis.

The objective of this research is to investigate the use of thermal catalytic pyrolysis as a route to the controlled synthesis of discrete silicon nanoparticles (powders). Due to its simplicity and the relatively straight-forward construction of the hot wire pyrolysis apparatus, the focus of this research is on determining its suitability for Si nanoparticle production. In chapter 2, various synthesis techniques suitable for Si nanoparticle production will be investigated and discussed. In chapter 3, special emphasis will be given to hot wire chemical vapour deposition (HWCVD) to show its reliance on thermal catalytic pyrolysis, and making use of the literature to determine its possible suitability for particle production. The broad parameters used in HWCVD of Si films will form the basis of the design and assembly of a particle synthesis system (reactor), which will be discussed in chapter 4. The processes followed for the set of experiments, with variations in the key parameters of operating pressure and hydrogen dilution, as well as

University of Cape Town

the characterisation techniques applied will be discussed in chapter 5. Finally, the as produced material will be characterised for morphology (size, etc), crystallinity and composition, and the results discussed in chapter 6.

University of Cape Town

2. OVERVIEW OF NANOPARTICLE PRODUCTION METHODS

In nanoparticle synthesis, the challenge is to control the production parameters to synthesise particles with the desired morphology, composition and properties (electronic, optical, electrical, magnetic, chemical and mechanical) [4]. A further challenge is the elimination of agglomeration and aggregation. Aggregation is irreversible particle sintering or clustering [9,10], which can be restricted by controlled powder synthesis and by suspending or dispersing the nanoparticles in a medium [1]. Agglomeration is particle adhesion due to van der Waals forces [9] and depends primarily on the number of particles (concentration) and their mobility. Both of these increase as particle sizes decrease [11].

It has been widely accepted that there are two major approaches that can be followed to synthesise nanoparticles. In the 'top-down' approach, the particles are formed by removing pieces from a bulk of the same material through breaking, electron or laser bombardment and etching. The end product is much smaller than the precursor. In the 'bottom-up' approach, atoms and molecules react with each other to assemble or agglomerate in a particle which is generally larger than the precursor. Further discussion on this approach will focus on mechanical processes, gas phase synthesis, vapour deposition and colloidal or liquid phase methods. The characteristics of particles synthesised may vary substantially, depending upon the technique used [11].

University of Cape Town

2.1 'Top-down' production

In top-down production the bulk material is reduced to nanoparticles by structural fragmentation, which may be combined with a solid state chemical process such as oxidation chemical reduction. Techniques mostly involve ball milling, laser ablation, sputtering and chemical etching.

Ball milling

Due to its simplicity, relatively inexpensive equipment, ease of up-scaling and applicability to almost all materials, ball milling has been extensively used to make nanoparticles. The challenge is to achieve mono-dispersion and prevention of contamination. Nanophase silicon powder can typically be produced by milling N-type and P-type single crystalline material in the form of grown silicon wafers or bulk silicon metal, milled to 50-100 nm particle size [12]. The size of the particles is however normally too large to exhibit quantum confinement effects. Solid phase reactions offer a way to produce silicon nanoparticles with reduced size (5-15 nm) [13]. The milling process, with the reaction $C + SiO_2 \rightarrow Si + CO_2$, may however take up to 240 hours, and a delicate further chemical process is required to separate the particles from the reactant [14]. In another approach, high purity aluminium powder is used as a reducing agent in the milling of SiO_2 [14]. The solid state reaction $3SiO_2 + 4Al \rightarrow 3Si + 2Al_2O_3$ produces nanosized crystalline silicon particles of 50 to 200 nm in a ball mill over a 24 hour cycle.

University of Cape Town

Laser ablation synthesis

Another often used top down route of producing nanoparticles is laser ablation, typically using pulsed Nd:YAG and excimer lasers with a typical pulse length of 25 ps [5]. The laser heats a small area of substrate material, resulting in the formation of an energetic plasma and supersaturated vapor above the substrate [15]. Particles form by interaction and condensation inside the vapour. Variation of the laser pulse frequency [16], backing gas type, and pressure result in nanoparticles with controllable size distributions. The material ablation rate decreases with longer target exposure times, and therefore the target is usually rotated. Although this method can generally only

produce small amounts of nanoparticles, in the range of 5 to 100 nm, laser ablation can vaporize materials that cannot be readily evaporated.

Etching

Highly uniform silicon nanoparticles, in the 1 to 5 nm range, can be produced by electrochemical etching of bulk silicon. A silicon wafer is gradually and slowly dipped into a hydrogen fluoride or hydrogen peroxide solution in the presence of an external current originating from a platinum cathode. The current density will determine the particle size formed [17].

Sputtering

In sputtering, an inert gas is ionised by a high voltage potential resulting in the ions being accelerated towards a precursor metal target. The sputtered material released on impact will form a supersaturated vapour that will condense upon cooling. This technique has been used to produce Si nanopowders in a hydrogen-rich plasma and are reported to resemble particles produced by chemical vapour decomposition of hydrogen-diluted precursors [18]. In another sputtering process, condensates were collected directly from the cold surface of a liquid nitrogen trap [19].

Spark synthesis

Nanoparticles can be created by a high-current spark between two electrodes of materials with high melting points, such as silicon [5]. The reproducible process generates only a small amount of nanoparticles [15] but, in the absence of an inert gas, is suitable for oxide production [20].

University of Cape Town

2.2 'Bottom-up' production

In bottom-up production the precursors are chemically different species, usually in the form of a liquid or gas. Through chemical reactions, nucleation condensation and agglomeration, solid particles are formed, that are physically larger than the individual constituents of the precursors. In general "bottom-up" production methods can be grouped into two classes, wet or colloidal chemistry and vapour phase synthesis as described below.

Colloidal chemistry

The basic principle of wet chemical synthesis of nanostructured materials is to initiate chemical reactions, and to control the nucleation and growth of the reaction products. As the particles are already in suspension, this route offers a good control of quality and reduced agglomeration, through the design of inter-particle forces. Furthermore nanoparticles can be made to tight tolerance specifications (mono-dispersed), and the chemical composition and morphology can be closely controlled. The disadvantage of liquid-phase processes is that washing, drying, and calcining are often required [21]. As an example, hydrogen terminated silicon nanoparticles can be produced by the reaction of Mg_2Si and $SiCl_4$ [22], but due to the numerous temperature regimes, reflux stages and drying cycles, synthesis takes longer than 2 days to complete. In another process, silicon nanoparticles in the 1-5 nm range are produced by reacting Zintl phase precursors with silicon and various solvents to produce group IV nanocrystals with passivated surfaces [23]. Similarly, a convenient one-step process, based on the thermal reduction of N, N'-di-tert-butyl-1,3-diaza-2, 2-dichloro-2-silacyclopentane in the presence of trioctylphosphine oxide and Li metal, has been reported to produce silicon particles in the 5 nm diameter range [24].

Vapour phase production

The process of chemical vapour synthesis has great flexibility in producing a wide range of materials and can take advantage of the huge database of precursor chemistries that have been developed for related CVD processes. The precursors can be solid, liquid or gas at ambient conditions, but are normally delivered to the reactor as a vapor [15].

University of Cape Town

Most, but not all, nanoparticle synthesis methods in the gas phase are based on homogeneous nucleation of a supersaturated vapour, and subsequent particle growth by condensation and coagulation [5]. Supersaturation is the state of any vapour whose pressure exceeds that at which condensation usually occurs at the prevailing temperature [10]. Immediate quenching is favourable for the formation of small particles [15] and limiting aggregation [5].

When continuous film growth occurs through chemical reactions at a substrate, the process is generally referred to as chemical vapour deposition (CVD). Most vapour phase production is suited to a continuous process, unlike colloidal synthesis that is carried out in batches, and takes hours to days to synthesise [15]. Furthermore, among all the synthesis techniques, gas-phase synthesis is one of the best techniques with respect to size mono-dispersity, typically achieved by using a combination of rigorous control of nucleation-condensation growth, and avoidance of coagulation by diffusion and turbulence, as well as by the effective collection of nanoparticles [4]. A closer look at a number of vapour phase process, with emphasis on silicon nanoparticle production, follows below.

1. Furnace pyrolysis

In this approach, vapor phase precursors are brought into a hot-wall reactor under conditions that favour nucleation of particles in the vapor phase rather than deposition of a film on the wall.

2. Spray pyrolysis

In spray pyrolysis, very small droplets of precursor solution are injected directly into the hot furnace. In this simple process, reaction often takes place in solution in the droplets, followed by solvent evaporation. High concentrations of non-agglomerated Si nanoparticles having diameters in the range of 10-40 nm can be produced with this method [25]. The size of the particles can be adjusted by controlling the initial precursor concentrations used in the spray. Furthermore, compared to calcined sol-gel-derived powders, particles produced by spray pyrolysis are more crystalline and less agglomerated [21].

University of Cape Town

3. Flame pyrolysis

Flame reactors are one of the most common reactor designs for the production of high-purity, mostly oxide, nanoscale powders in large quantities. The flame provides the energy to evaporate the precursors and to drive the chemical reactions. Powders, liquids or vapours can be used as precursors. Due to the high energy density in the flame, the precursor can reach temperatures as high as 2400 °C which is crucial for primary particle formation [4]. The coupling of the particle production to the flame chemistry, however, makes this a complex process that is rather difficult to control [15], which although inexpensive, usually yields agglomerated oxide particles [5]. This process often relies on the rapid quenching of the flame aerosols to rapidly slow down particle growth downstream of the nozzle, thus preserving the particle size and morphology of the upstream aerosol [26]. Due to the flame chemistry the technique is not suitable for silicon nanoparticle synthesis, but has been used for silicon oxide powders in the 15 to 20 nm size range [9].

4. Laser Pyrolysis

Laser pyrolysis allows highly localized heating and rapid cooling of the reactant gas. Heating is generally done using an infrared (CO_2) laser, whose energy is absorbed by either one of the precursors or an inert photo sensitizer, such as sulphur hexafluoride. Gas-phase decomposition of the reactants takes place due to the temperature increase, and supersaturation is created, resulting in nanoparticle formation. SiH_4 pyrolysis results in Si nanoparticle formation [5,15,27]. The process allows good control of the composition, shape and size distribution of the resulting powders [28], and, dependant upon the parameters, may lead to high-purity silicon crystallites with diameter between 2 and 20 nm [29], or to amorphous particles with similar size distribution [30].

5. Plasma pyrolysis

Yet another means of providing the energy needed to induce reactions, which lead to supersaturation and particle nucleation, is to inject the precursors into a thermal plasma. This generally decomposes them fully into atoms, which can then react or condense to form particles, when cooled by mixing with cool gas or expansion through a nozzle [15]. Pure single crystalline silicon nanoparticles can be produced by microwave

University of Cape Town

induced plasma pyrolysis of SiH_4 in a low pressure flow reactor. The reactor consists mainly of a quartz glass flow tube, into which the premixed reaction and dilution gases (SiH_4, H_2, Ar) are injected. The microwave energy is coupled into the gas flow, forming flame-like plasma. Particles with diameters in the range 6 to 11 nm are produced by controlling the precursor concentration, gas pressure, and microwave power. The benefit of this technique is its relative simplicity and its scalability, which allows it to deliver macroscopic amounts of nanophase material. Silicon nanoparticles produced in this way are crystalline [31] and usually isolated and spherical in shape [32].

6. Hot wire chemical vapour deposition (HWCVD)

HWCVD involves the decomposition of a precursor gas at a heated catalyst, usually a wire or filament, producing radical species which react in the gas phase, and deposit onto a heated substrate. In the case of higher pressure, gas phase nucleation and particle growth is possible. HWCVD is a suitable deposition technique for preparing various devices and thin films, which can be superior to devices made with conventional plasma enhanced CVD [33]. High-efficiency a-Si:H solar cells and high performance thin-film transistors can be produced. At the same time, the technique is much simpler to set up and control than any of the other techniques mentioned [34]. The key parameters in synthesis with HWCVD are: pressure, filament temperature, substrate temperature, and precursor flow rate, dilution of the precursor with hydrogen or other gases as well as system geometry. HWCVD will now be discussed in more detail in chapter 3.

University of Cape Town

3. HOT WIRE CHEMICAL VAPOUR DEPOSITION

In the previous chapter, a number of possible nanoparticle production techniques have been discussed. In this chapter the focus will be on the HWCVD technique, and its possible use for the synthesis of silicon nanoparticles.

HWCVD is primarily used for the deposition of thin films and thin film electronic devices. Applications include the production of high performance thin film transistors [34], high-efficiency solar cells [33] and silicon nanowires [35], as well as various other devices with a performance that can be superior to devices made using conventional plasma enhanced CVD (PECVD) [36]. Other applications of HWCVD include protective coatings such as a-C:H [37] and Teflon [38].

HWCVD of silicon saw its birth in 1979, when Wiesmann et al. [39] reported a method which could produce hydrogenated amorphous silicon (a-Si:H) films at high deposition rates. But the electronic properties of films produced were inferior to films grown by PECVD. The technique was thus not really pursued until 1985, when Matsumura et al [40] demonstrated hydro-fluorinated amorphous silicon films of high electronic quality, using silicon difluoride and hydrogen precursors. A year later Matsumura produced high-quality a-Si:H under similar deposition conditions [41], and called the process "catalytic CVD" , believing that the reaction of the hydrogen and silane, at the hot filament is catalytic. In 1988, Doyle et al [42] also grew high-quality a-Si:H under similar conditions, naming their process "evaporative surface decomposition", due to the efficient decomposition of a low-pressure source gas by the filament, to produce deposition radicals. The process was later renamed "hot-wire assisted CVD" by Mahan et al [43], who thoroughly compared a-Si:H grown by HWCVD with that grown by PECVD, leading to renewed research activities and interest in the technique. Compared with the extensive research in physical vapour deposition (PVD), there has been less work on understanding the initial stages in chemical vapor deposition (CVD) processes,

University of Cape Town

despite the technological and commercial importance of CVD-based manufacturing systems [44].

The HWCVD technique is much simpler to set up and control than any of the other techniques mentioned [34], and can also be scaled up easily. Uniformly deposited a-Si:H films of over 1 m^2 have been reported [34]. But, although hydrogen terminated silicon is an attractive starting point for the synthesis of novel modified silicon surfaces, little investigation has been done on hydrogen terminated silicon nanoparticles [22].

3.1 The HWCVD process

University of Cape Town

As illustrated in Figure 3.1, HWCVD is a technique that involves the decomposition of a precursor gas on a heated refractory metal filament, to produce radical species, which are believed to be responsible for thin film growth (Figure 3.1 (a)) on a heated substrate. Under certain conditions radicals might also react in the gas phase and, through nucleation, condensation and agglomeration are believed to grow into nanoparticles, or produce low quality films (Figure 3.1 (b)).

The filament not only supplies the heat for the precursor pyrolysis, but also has a catalysing function. Tungsten and tantalum are the materials most often used as filaments. The dissociation rate of silane directly depends on the filament temperature [45], with a minimum temperature identified for silane dissociation at 1400 °C [42]. Dissociation may increase significantly if the temperature exceeds 1500 °C [33]. At low temperatures, the silane will react with the metal of the filament, forming silicide on the surface. This affects the filament resistance, making it difficult to reproduce the process, and may lead to premature wire breakage [34].

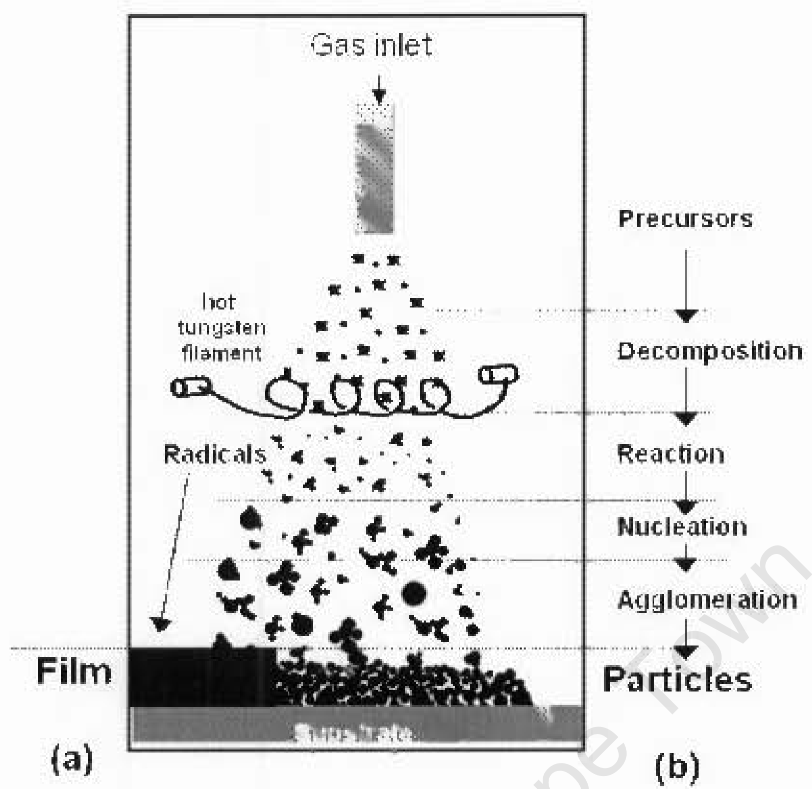

Figure 3.1: Hot wire CVD process forming (a) thin films from radicals and (b) particles from vapour phase reactions and nucleation.

University of Cape Town

The dissociation by the catalytic filament produces a number of species, including radicals, in the gas phase. These may further react in the gas phase, with some common reactions being [45]:

$H + SiH_4 \rightarrow SiH_3 + H_2$

$H + SiH_3 \rightarrow SiH_2 + H_2$

$SiH_3 + SiH_3 \rightarrow SiH_4 + SiH_2$

$Si + SiH_4 \rightarrow Si_2H_2 + H_2$

$Si_2H_2 + SiH_2 \rightarrow Si_3H_4 + H_2$

It should be noted that the full list of possible vapour phase reactions, including clusters and leading to particle formation, has been extended, to 33, through numerical investigations [46]. At the same time 14 surface reaction mechanisms, including silanes, silylenes, silicon hydrides and silicon clusters have been suggested [46]. Research into vapour phase reactions and particle production is ongoing.

During the initial stage of film deposition, radical species adsorb onto the substrate surface as adatoms, diffuse, and then either aggregate with other adatoms, to create new islands, or are captured by existing islands to cause island growth. Defects on the substrate, may trap the diffusing adatoms and additionally, islands can be mobile, deform their shape, and dissociate [44]. The quality and characteristics of the layers greatly depends on variations in the HWCVD parameters. These parameters are pressure, filament temperature, silane dilution ratio (with H_2) and substrate temperature, each of which is briefly discussed below:

- **Pressure**

The pressure directly effects layer quality. In general, if the pressure is low enough, the reactive species are transported to the substrate without gas-phase particle formation, which leads to denser and higher quality films [33,47]. At higher pressure, there will be more gas-phase interaction, leading to porous films with poor quality. The deposition rate can also be linked to pressure and is reported to be low at low pressure, increases with medium pressure (0.1 mbar) and then decreases at high pressures (>4 mbar) [48].

- **Filament temperature**

In combination with favourable choices of other parameters, the filament temperature can be directly linked to the properties of the films deposited. In general amorphous material will be deposited for filament temperatures lower than 1650 °C and nanocrystalline material at filament temperatures higher than 1750 °C [49].

- **Hydrogen dilution ratio (H2:SiH_4)**

In general, a consistent enhancement of the crystallinity can be achieved with increase in hydrogen dilution ratio [50], while amorphous layers are generally obtained in pure silane or in low dilution [47].

- **Substrate temperature**

High temperature substrates (>300 °C) promote denser film growth and increase crystallinity. A decrease in the substrate temperature (<200 °C) promotes an increase in the hydrogen content and a lower sub-gap absorption in a-Si:H [47], and may lead to

University of Cape Town

layers that are disordered, and highly defective. The dominant defects can be micro voids, decorated with hydrogen, in contrast to the smaller dangling-bond defects seen in high-temperature grown samples [51].

	Lower range (Film properties expected)	**Higher range** (Film properties expected)	**Suggested favourable conditions for particle growth**
Pressure (operating)	***(μbar - range)*** Dense [47] Crystalline [48] Low deposition rate	***(mbar - range)*** Porous [47] Amorphous High deposition rate [48]	Higher pressure
Filament temperature	***(1400-1600°C range)*** Amorphous [52] Filament degradation	***(1600-2000°C range)*** Crystalline [52]	High temperature
Hydrogen dilution	Slow growth rate Amorphous [47]	Fair growth rate Crystalline [47] [50]	Full range to hopefully control crystallinity
Substrate temperature	(< 300 °C range) Disordered and defective [51]	(> 300°C range) Dense	Low, if possible room temperature or cooled, to prevent film growth.

Table 3.1: General tendency of thin films to acquire properties under the mentioned conditions

The parameters, and their effect on film properties, can be summarised in the form of a table (Table 3.1). Due to the many combinations of these parameters, and variances in results, only the general tendency of the films to acquire specific properties under lower and higher parameter values is given.

3.2 HWCVD for nanoparticle synthesis

The overview has shown that HWCVD is a suitable deposition technique for preparing thin films with good performance. But, almost without exception, the focus of HWCVD research published has been on understanding and improving thin films, and not on nanoparticle synthesis. An interesting exception from this focus has been the report of the formation of powder as a frequent by-product of silicon chemical vapor deposition (CVD), due to gas-phase chemical reactions that lead to homogeneous nucleation [53]. Of further interest is the theory of charged clusters (TCC) proposed by N.M. Hwang [35,54-56], which suggest that the formation of many thin films is not as a result of

University of Cape Town

atomic deposition, but rather by the gas phase formation of nanoclusters, that form the growth particle of the thin film. In another experiment by the same group [57], it is suggested that neutral clusters attach themselves on to the growing surfaces randomly by Brownian coagulation, leading to highly porous skeletal structures, or the so-called "snowing" phenomenon.

The relative simplicity of HWCVD [34], as well as the references above, could be seen as supporting the hypothesis, that silicon nanoparticles, in powder form, can be synthesised with HWCVD equipment. Since this research is no longer concerned with film deposition, but with the production of nanoparticles through gas phase pyrolysis, a more appropriate name for the technique is thermal catalytic pyrolysis (TCP). To help with the specification of this system, the minimum and maximum parameter values, gained from the literature are summarised in (Table 3.2). The last column indicates the range to be considered.

	Minimum	**Maximum**	**Range considered for system**
Pressure (operating)	10 μbar	66 mbar	30 μbar – 30 mbar
Filament temperature	1400 °C	2000 °C	1500-1900 °C
Flow rate (total)	10 sccm	200 sccm	10-100 sccm
Hydrogen dilution	0%	97%	0-90%
Substrate temperature	200 °C	850 °C	As low as possible
Filament	0.25mm (W), 0.25mm (Ta)	0.5mm W	0.5mm W

Table 3.2: Minimum and maximum parameters as reported in the literature and range to be considered for the system to be assembled

In the next chapter the design and construction of a TCP system will be discussed in detail. Furthermore, the system will be tested under production conditions and its performance, will be evaluated and discussed.

University of Cape Town

4. THERMAL CATALYTIC PYROLYSIS SYSTEM

In the chapter 3, the possibility of using thermal catalytic pyrolysis (TCP), as a production method for silicon nanoparticles was investigated. A vacuum system with gas supply, reaction chamber and instrumentation, is now required to test the suitability of the TCP process for silicon nanoparticle production. In this chapter, the design and construction of a TCP system, as well as its performance, will be discussed.

Before starting with the design and assembly of the system, the operating pressure, filament and substrate temperature, as well as hydrogen dilution need to be considered. The considerations discussed in chapter 3, see Table 3.2, offer some guidelines. For thin films, depositions have been made with the precursor ranging from 100 % silane, to a hydrogen dilution as high as 97% [58], and sometimes the silane is diluted with He [59]. Operating pressures may vary from 10 μbar or lower [60], up to 66 mbar [47]. Flow rates may be as high as 200 sccm [61], but are mostly in the 20-60 sccm range [33]. The literature, in general, shows that both tungsten and tantalum filaments of 0.25 to 0.5 mm diameter are most often used. The filament temperature is usually not lower that 1500 °C [52], or higher than 2000 °C [60] but is most often between 1600 – 1800 °C [33], while substrate temperatures of 300 – 850 °C [47] are reported. It appears that Corning 7059 glass is frequently used as a substrate, although various orientations of silicon are also reported, depending on the application.

After consideration of the process conditions above, the system is designed for a pressure of 0.03 to 30 mbar, a filament temperature of up to 1900 °C and a flow rate of 10-100 sccm. The substrate, which only serves as a collector, will not be heated for the current research. Furthermore the basic components of the system will comprise a reaction chamber and vacuum system, gas supply and control, hot wire power supply, as well as other instrumentation.

University of Cape Town

In nanoparticle production, health and safety should be of primary concern. Toxic, flammable and potentially explosive precursors are not uncommon, and precautions must be in place to prevent and contain accidents. Silane, which is the predominant precursor for silicon deposition in many processes, is pyrophoric and will burn if in contact with air. A mixture of silane and hydrogen can form a highly explosive mixture if uncontrolled oxygen penetrates the chamber. Another risk is the toxicity of precursors, as well as possible by-products from chemical reactions. Materials safety data sheets [62], as well as possible chemical reactions of the species involved, should were studied carefully and precautions implemented to prevent accidents. Furthermore, the potential exposure to nanoparticles can pose a health risk. While liquid phase production will greatly limit the number of airborne particles [11] , the risk of exposure is expected to be greatest where nanoparticles are manufactured in the gas phase and harvested as a dry powder.

4.1 System overview

An effort was now made to assemble a system that satisfies the above requirements. The system as constructed will now be described, starting with the overall system diagram shown in Figure 4.1. Starting at the right of this figure, gas supply lines feed hydrogen and nitrogen from outside the building to the gas control console inside the laboratory. The silane line enjoys additional safety precautions, namely a stop valve at the cylinder and an additional stop valve where it enters the laboratory, and a connection to electrical earth lines. In order to flush the silane line after use, the nitrogen line, protected by a non-return valve, connects directly to the stop valve at the silane cylinder. As can be seen in the centre of Figure 4.1, all gases which are regulated to lower pressures and pass through flow meters (ABB Purgemaster Series A6100), connect to the gas manifold, which through a stop valve, connects to the gas inlet pipe at the reaction chamber. This is the only gas inlet into the chamber. To record, for safety purposes, the contents and pressure of the silane line, it has been colour coded (record sheet attached in Appendix A).

University of Cape Town

On the left of Figure 4.1, the reaction chamber (reactor) including the filament holder, substrate holder, shutter and carousel can be seen. From the bottom plate, the chamber connects to a pressure regulator valve, manifold and rotary vacuum pump at the bottom of the figure. Excess gas is released through the exhaust directly into the atmosphere, where the silane reacts with air to form silicon oxides. Instrumentation, shown in Figure 4.1 around the reactor, includes two pressure gauges, a thermocouple, the filament power supply, and the current and voltage meters.

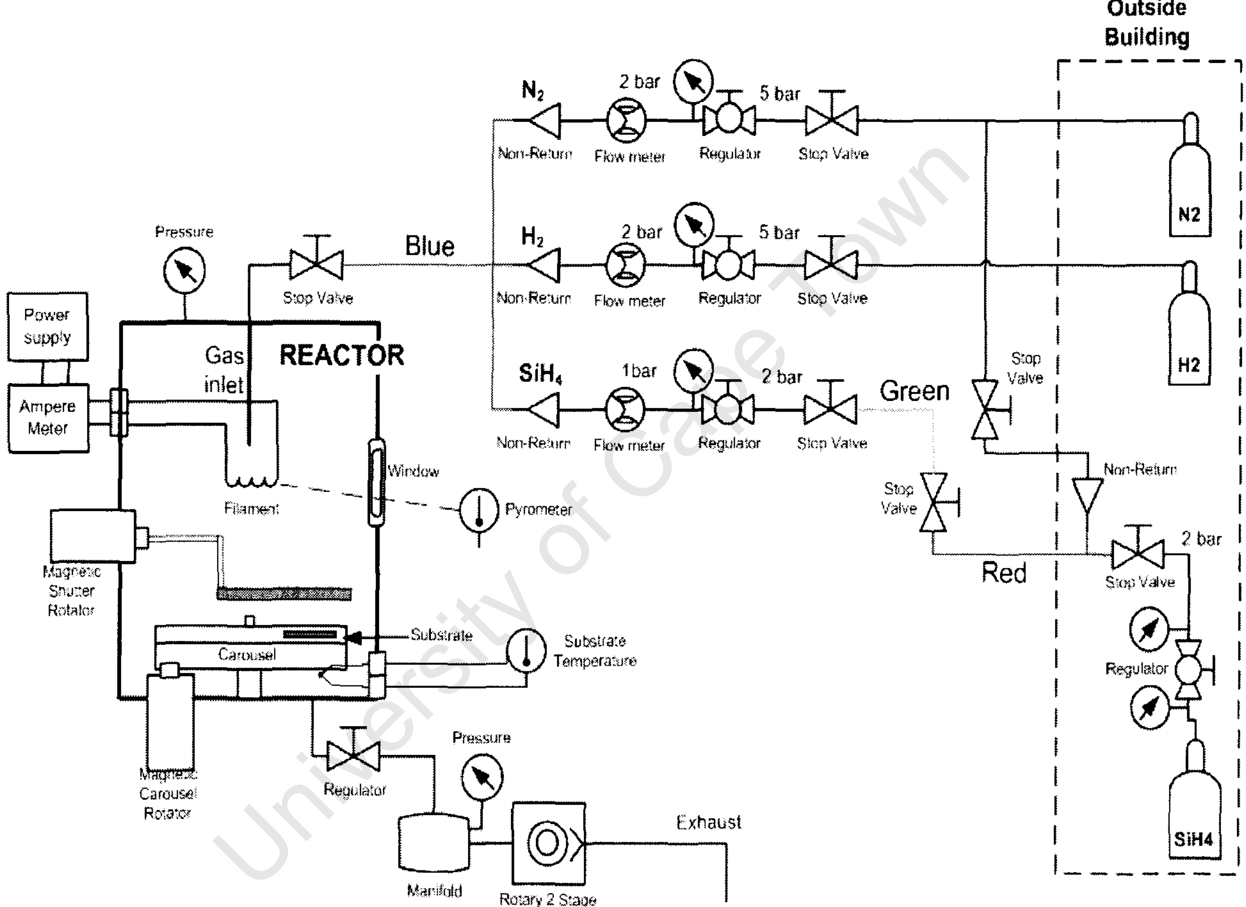

University of Cape Town

Figure 4.1: System diagram

Figure 4.2 shows the thermocouple readout unit, pressure gauge indicator, variable transformer and filament power supply for the system.

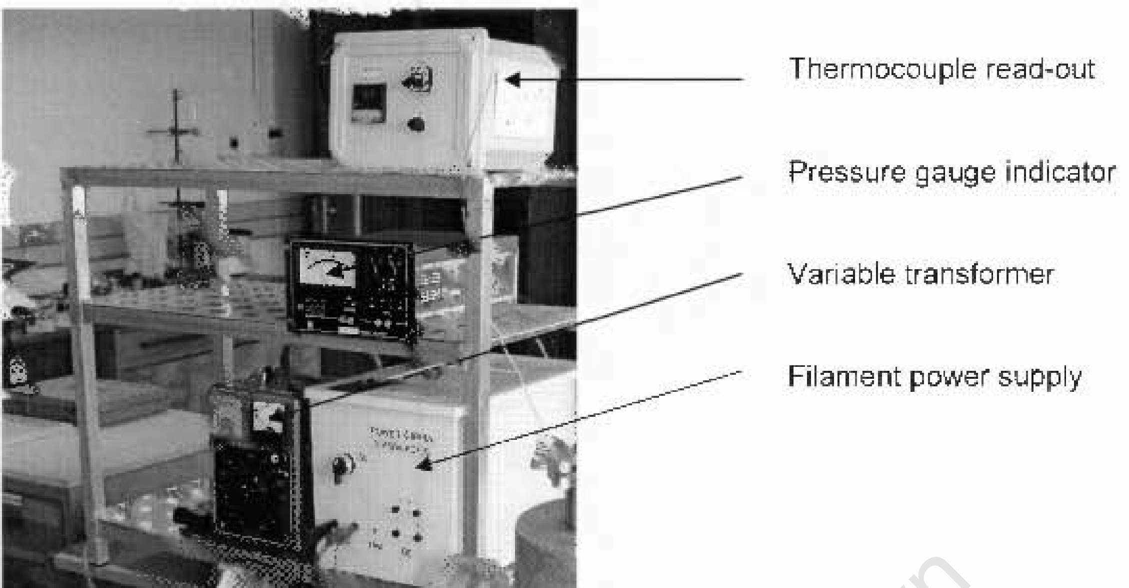

Figure 4.2: Instrumentation for system control

4.2 Reaction chamber

Before constructing and assembling the system, the material safety data sheet of silane [62] was consulted to determine safe handling of silane. The Scott Specialty Gases design and safety handbook [63] was also consulted to find out which materials may react with silane. Brass, stainless steel (303 and 316), aluminium, copper, PCTFE, Teflon, PVC, polycarbonate, Viton, Neoprene and polyurethane are listed as usable materials. A previously used, compact, stainless steel cylindrical chamber with inside diameter and height of 150 mm and volume of 2.65 litres is used for the reaction chamber as shown in Figure 4.3. There are two NW40 and two CF40 ports on the side of the cylinder. The CF40 flanges have been fitted with quartz view-ports, while the others are used for the filament holder and the shutter mechanism. Three more NW40 ports can be found at the bottom of the base plate, and two type NW10 flanges on the top of the cylinder. All flanges and entry ports to the chamber are sealed with Viton O-rings. As shown in Figure 4.3, the chamber is mounted between the gas control panel and the instrumentation rack, on a steel frame. Also shown, is the copper pipe which was wound around the chamber to cool it. The 14 turns of ¼ inch copper pipe are

University of Cape Town

wound around the chamber and connected to a water supply. A flow rate of 2 litres per minute cools the chamber to ≈ 30°C on the outside.

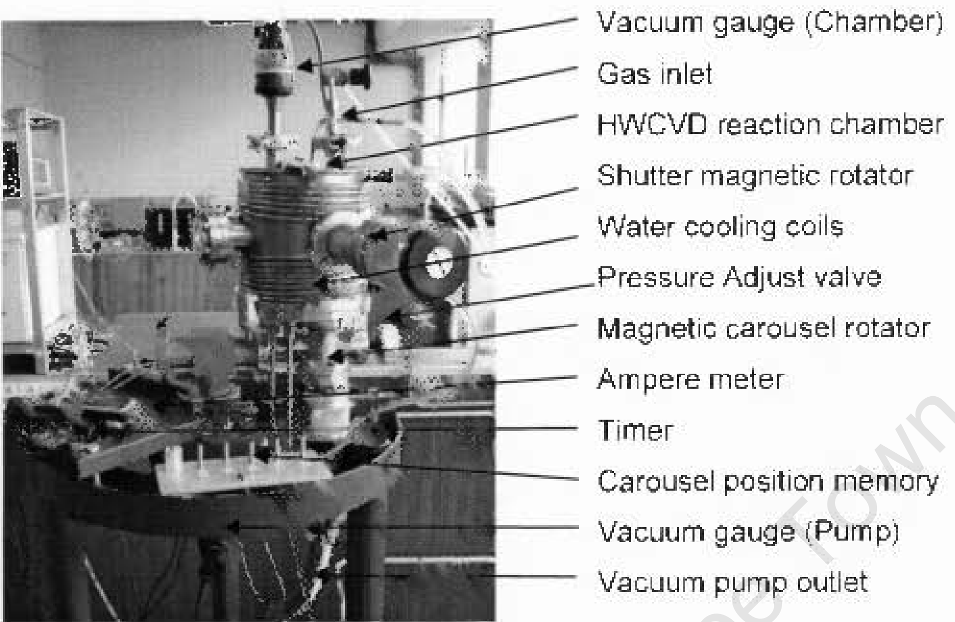

Figure 4.3: Reaction chamber and instrumentation

In Figure 4.4 the relative positions of the parts of the chamber are given. The two view-ports are not shown. The distance from the filament to the substrate is 50 mm, and to the base plate 80 mm, while the gas feed pipe which points directly at the filament is 30 mm from its centre. The NW10 flanges, at the top of the reactor, are used for the gas feed and for the vacuum gauge, while the flanges at the bottom plate are used for the vacuum pump connection, the carousel rotation, and the thermocouple feed-through. To deliver the precursor gas directly to the filament, a pipe is welded to a NW10 connector and slightly bent so that it reaches the centre of the chamber.

University of Cape Town

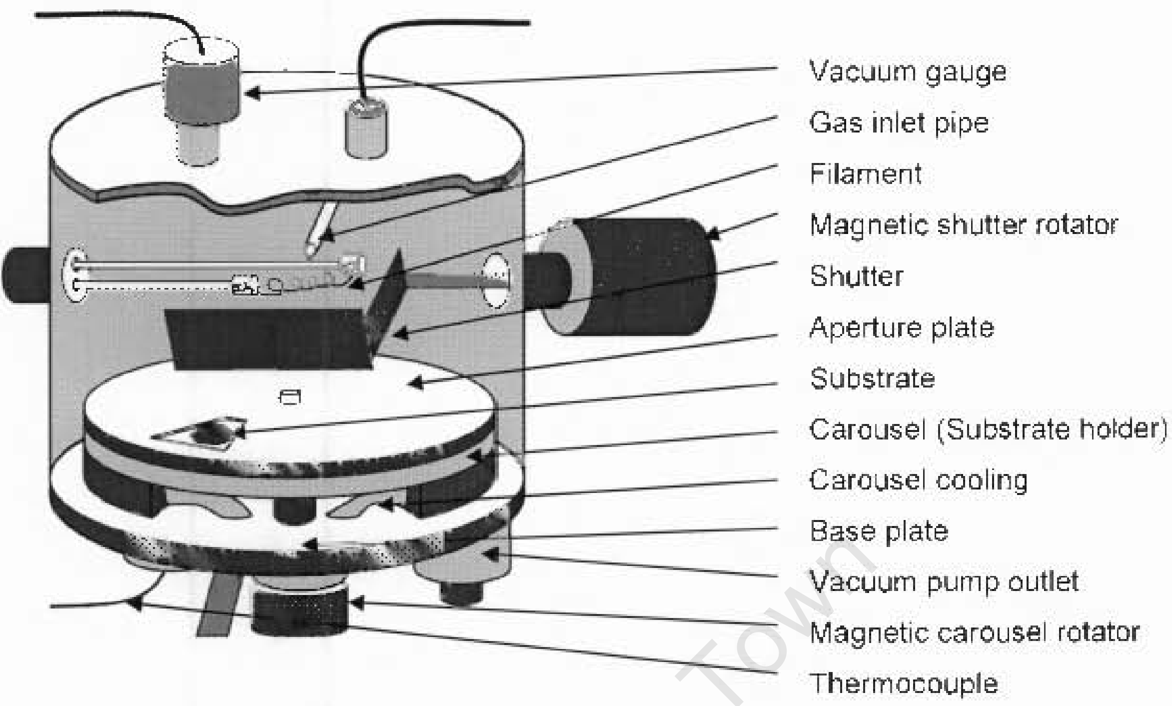

Figure 4.4: Reaction chamber functional drawing

At the bottom of Figure 4.4, the position of the magnetic carousel rotator, the carousel cooling pipes, and the thermocouple, as well as the vacuum pump outlet are clearly shown. As indicated in Figure 4.5, the ports on the side of the reactor are positioned at angular intervals of 120°, 105°, 45° and 90°, and their centre distances are all 80 mm from the bottom plate. The bottom plate ports can be found on a pitch circle of diameter of 80mm and are equally spaced at 120° intervals.

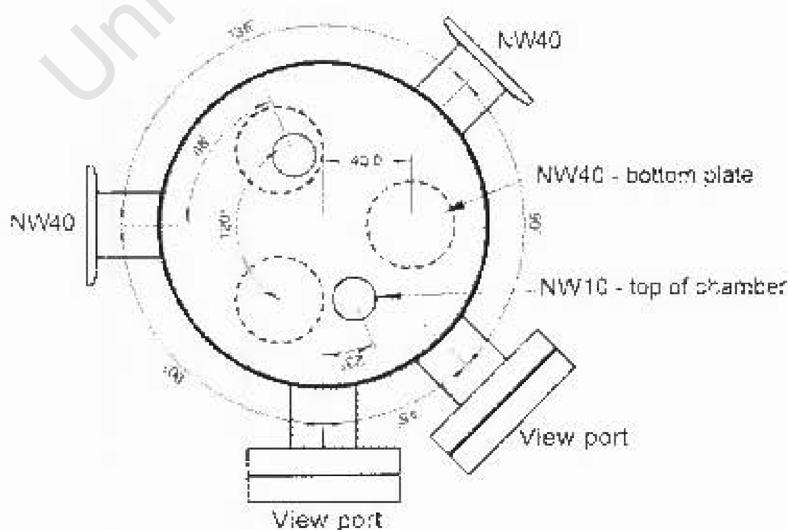

Figure 4.5: Top view of reaction chamber design

University of Cape Town

The main purpose of the shutter is to enable depositions under controlled conditions and time periods. The shutter is typically closed while the system is prepared for, or between, depositions. A circular sliding shutter, operated by moving a strong magnet on the outside, was initially used, but was later replaced with a rotating shutter, operated by a magnetic rotary feed-through. The shutter, as seen in Figure 4.6 is in the form of a wide, open spoon. In its open position (as shown), the shutter shields the view-ports from the filament and when closed shields the substrate.

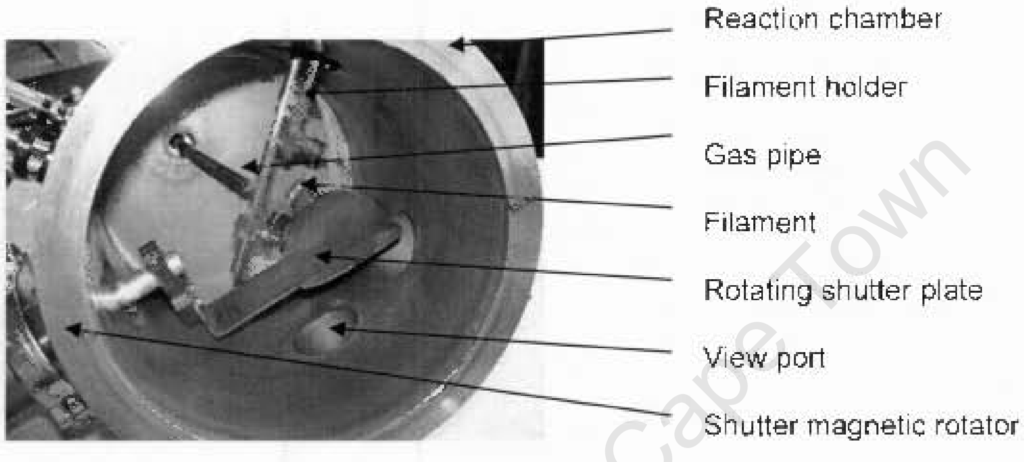

Figure 4.6: Filament, and shutter, and gas inlet relative positions

University of Cape Town

A filament holder, shown in Figure 4.7, was constructed by using an NW40 electrical feed-through flange, and mounting two stainless steel rods of 6 mm diameter, each to three of eight electrical contacts. Contact blocks with M5 screws, fasten the filament to these rods. A special connector, with 4 mm electrical (banana plug) sockets was cast in epoxy resin to for the outside of the electrical feed-through. Three parallel cables were found suitable to supply an AC current of up to 30 A to the filament. Markings on the matching flanges of the reaction chamber, filament holder, and gas supply pipe, ensure accurate positioning during assembly.

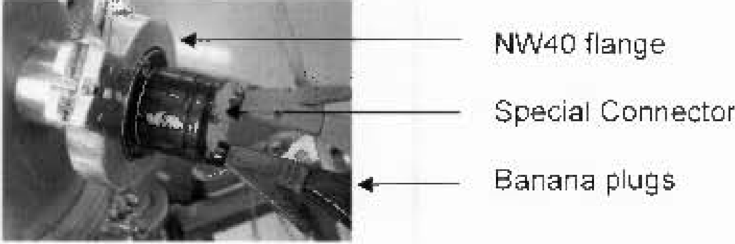

Figure 4.7: Electrical feed through into chamber

After investigating glass, silicon crystal, quartz, and stainless steel, the latter is used as a substrate. It is cheap, available, and easy to work and clean, and lends itself well for later up-scaling. Stainless steel plates (type 304 and 1.2 mm thick) were cut into octagons with 28mm, being the distance between any opposite sides. The substrates are numbered by punch marks on the bottom side of the plates. A numbering system, with 1 to 6 punches in the centre, and 1 to 6 punches on the side of the plate, allows the marking of 36 individual and identifiable substrates. Due to the fact that the substrate temperature strongly influences the film properties in HWCVD [45], and since this system is primarily aimed at the synthesis of powders or loose particles, the substrate must function as a collector plate only, and be maintained at a constant low temperature. After initial experimentation with a substrate holder for single substrates it was found (Figure 4.13) that the radiation of the filament substantially heats the substrate over time. The substrate holder thus has to be cooled. Furthermore, no load lock is available in the system to ease the interchanging of substrates. These considerations lead to the design and manufacture of the cooled carousel shown in Figure 4.8. It consists of a cooled carousel support, the carousel with 6 numbered substrate compartments, and the aperture plate, which covers all but one compartment and is in turn covered by the shutter (not shown here). A magnetic rotating feed-trough, connected through one of the bottom flanges, turns the carousel.

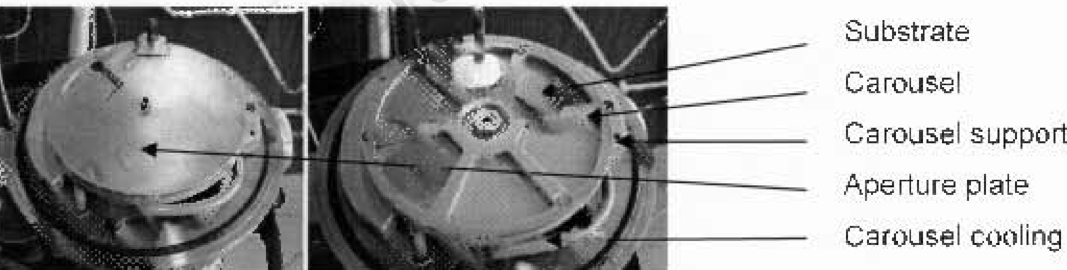

Figure 4.8: Carousel with (left) and without (right) aperture plate

A K-type thermocouple, protected in 2 mm diameter stainless steel tubing, penetrates the chamber through a 1/16 inch male NTP threaded pipe connector, which is fastened to a NW40 blank cover flange. The thermocouple is in direct contact with the bottom of the carousel at the position of the aperture. For temperature measurements of the chamber wall and single substrate, the thermocouple was extended and bent to reach the

new measurement location. A digital temperature controller (REX – S400 from RKC Instrument Inc.) is used as a temperature read-out.

4.3 Vacuum pump and gas handling

An Edwards E2M8 Rotary pump with 8 m^3h^{-1} pumping capacity is used, which achieves a minimum pressure of 4 x 10^{-3} mbar. To prevent reactions with the silane Alcatel 200 oil is used in the pump. Due to the explosion risk of the silane and hydrogen, the exhaust from the pump must be handled with care. A liquid trap and tube oven (800°C) were investigated, but a simpler solution proved to be safer to manage. A ½ inch stainless steel pipe is connected directly from the vacuum pump outlet to the outside, with a 90° downward bend at the end. In later tests with total flow rates into the reactor of up to 100 sccm, and 20 to 80% dilution with hydrogen, as well as cold to 1900°C filaments, the exhaust performs well and safely.
The flow rate recorded by the flow-meters is dependant on the viscosity, temperature and pressure of the specific gas. For silane the standard values are: 1.08 x 10^{-4} Poise, 21°C and 2 bar, respectively. Calibration data (CD Calc version 13.03) was used to make replacement gauges for the flow meters, which make it easier and safer, to manually set and maintain the desired flow rate during the synthesis. Table 4.1 indicates the new meter values as calculated.

University of Cape Town

Original scale on flow-meter	**New scale calibrated for gas**		
	Φ_{N2} (cm^3/min)	**Φ_{H2} (cm^3/min)**	**Φ_{SiH4} (cm^3/min)**
3	3.8	3.8	2
6	41	41	21.5
9	99	119	58

Table 4.1: Mass flow meter calibration table

4.4 Filament and power supply

As discussed in chapter 3, the hot filament is the key component in HWCVD systems. Both tungsten and tantalum have been reported as suitable catalytic materials, but usually 0.5mm diameter tungsten wire, mounted straight, in a coil [64] or even a basket [49] is used. The spiral shape of a coil allows a longer wire per volume, and may reduce stress in heating and cooling cycles, and furthermore minimises the sagging effect [34]. For this system a 0.5mm diameter tungsten wire of 99.95% purity is used. The wire typically contains, in parts per million, by weight: Al 10, Ca <10, Cd <2, Cr <5, Cu <10, Fe 20, K 50, Mg <4, Mo 40, Na 5, Ni <10, Rb 2, Si 45, H 3, N 6, O 15, S 5 [65].

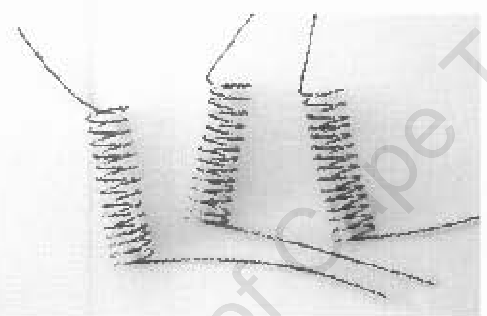

Figure 4.9: As manufactured tungsten filaments

Filaments (Figure 4.9) are constructed by winding 14 turns of tungsten wire onto an M6 thread, yielding repeatable products, with inside diameter of 6 mm, a width of 16 mm and total wire length of 30 ±5 mm. The filament is directly mounted on 2 stainless steel rods with diameter 6 mm, and the rods are directly fastened to an NW40 electrical feed-through. The length and position of these rods puts the filament in the centre of the reaction chamber, and in full view of the view ports. This is important, as the pyrometer, used to determine the filament temperature, requires line of sight.

The filament has a low resistance, which requires a high current and low voltage power source to heat. To define this power supply for the filament, rough indications of current and voltage will be calculated. A wire length of 25 mm and temperature of 1700 °C will be used in calculating the resistance from first principles. Energy losses due to convection and chemical reactions in the chamber will not be taken into account.

University of Cape Town

Firstly, the wire resistance (in Ω) at room temperature for a length L is calculated from

$$R = \rho \frac{L}{A} , \qquad (4.1)$$

where A is the cross section area (19 x 10^{-8} m^2), and ρ is the resistivity (5.6 x 10^{-8} Ωm for tungsten) of the filament material. This gives a value $R = 0.0737\,\Omega$.

It is now possible to calculate the wire resistance R_2 at the operating temperature T_2, using:

$$R_2 = R_1(1 + \alpha(T_2 - T_1)) , \qquad (4.2)$$

where α is the temperature coefficient of resistivity (0.0045 °C^{-1} for tungsten), and T_1 is the temperature at which the resistance (R_1) is known. At 1700°C, $R_2 = 0.63\,\Omega$.

The power required to heat the filament to the operating temperature is calculated using the Stefan-Boltzmann equation [66]. The energy radiated from the filament is

$$\frac{\Delta Q}{\Delta t} = \varepsilon \sigma A T^4 , \qquad (4.3)$$

where ε is the emissivity (0.44 for Tungsten at 21 °C) and σ the Stefan-Boltzmann constant 5.67x10^{-8} $Js^{-1}m^{-2}K^{-4}$. A is the surface area of the filament, and T the temperature in Kelvin, and $\frac{\Delta Q}{\Delta t}$ is the power needed to maintain the filament at the given temperature. The result is 145 Watt.

The equation $I = \sqrt{\frac{P}{R}}$, derived from Ohms law ($P = IV$) results in a current of 15.2 A at a voltage of 9.6 V. These two values define the required power supply.

University of Cape Town

A simple AC/DC power supply is constructed (Figure 4.10) from a used 500 VA transformer, with a capability of 20 A at 25 V, up to 50 A at 10 V, maximum. To control the filament temperature a 1 kW variable transformer is connected to the input of the power supply. A change in voltage on this variable transformer leads to a change in voltage and current in the filament, which leads to a change in temperature. The details of the design will not be discussed in detail.

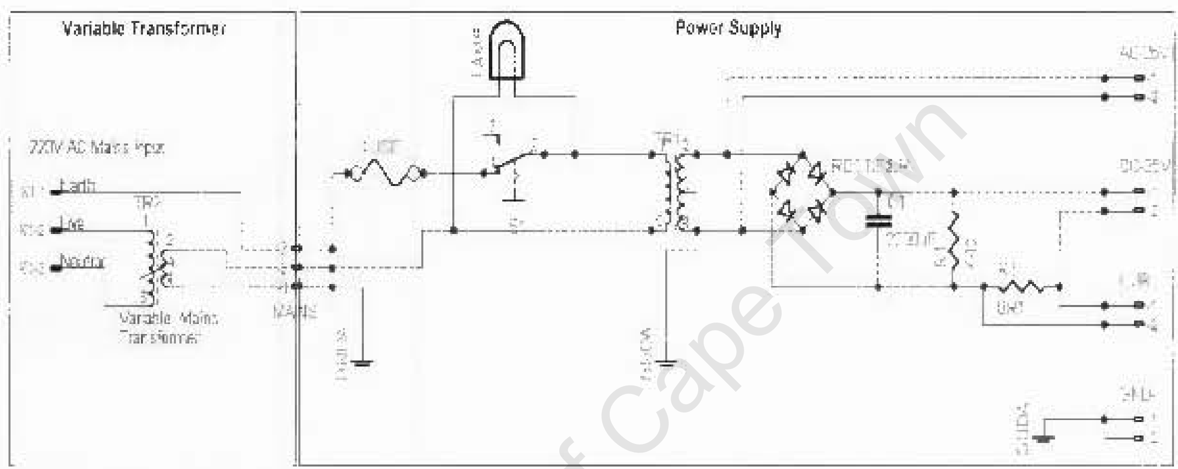

Figure 4.10: Schematic diagram of the as-built power supply

University of Cape Town

The performance of the constructed power supply was tested experimentally, and it achieves a maximum alternating current of 18 A for a 25 mm tungsten wire and due to the potential losses in the rectifier circuit (≈ 4 V) a maximum direct current of 17 A.

4.5 System performance

Filament Temperature and Current Ratio

It has been reported [34,45] that the current of a filament in HWCVD systems is directly proportional to the temperature. In the system constructed, the filament temperature is controlled by regulation of the current through the filament, using the variable transformer. An experiment was conducted to determine the temperature vs. current

characteristics of the 0.5 mm diameter tungsten wire coiled filament. The experimental setup is shown in Figure 4.11.

A Land/Minolta Cyclops 52 pyrometer, with 600-3000 °C temperature range, accuracy of ±0.5% of reading, and spectral response of 0.8 - 1.1 μm is used. It is a single wavelength instrument, which means that the emissivity of the wire must be taken into consideration. The instrument had previously been calibrated against blackbody radiators over the range 600 °C to 1600 °C at 1.2 m distance, with an emissivity setting of 1. The transmittance of the quartz window of the reaction chamber was measured with a Perkin Elmer Lambda 35, UV/Vis scanning double-beam Spectometer, to be 93% at these wavelengths.

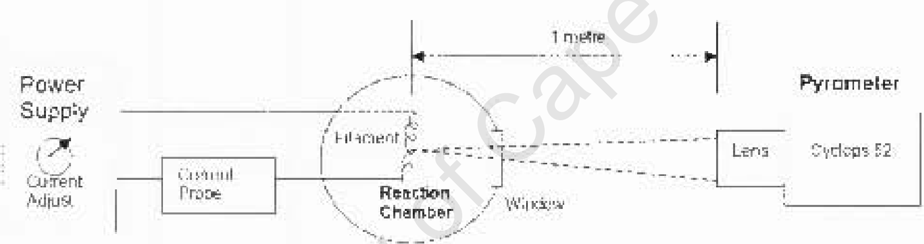

Figure 4.11: Setup for the current vs. temperature calibration for the filament

The pyrometer was positioned on a stable tripod, one meter from the filament, with the red filter fitted. The emissivity of elemental tungsten was taken as 0.44, but the instrument was set to 0.43 to compensate for the absorption in the quartz window. The gas in the chamber was nitrogen and the filament was heated by alternating current. Four sets of measurements were taken at different pressures, from 0.3 mbar to 30 mbar, and the average temperature determined and plotted in Figure 4.12. To see the trends more clearly, data points have been connected. The temperature drops slightly with an increase in pressure.

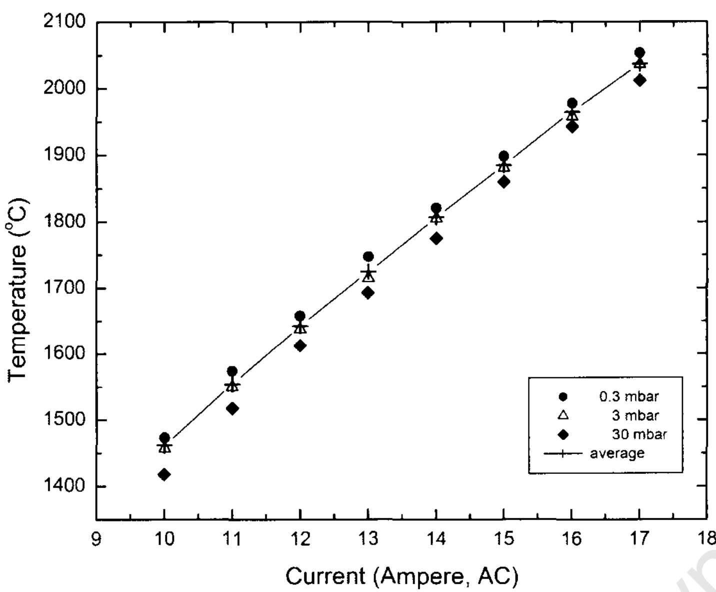

Figure 4.12: Temperature vs. Current Characteristics

Figure 4.13 shows the heating effect of the filament over time, as measured on a single substrate, the reactor wall, and on the cooled and un-cooled carousel. The measurements were performed under operating conditions of 0.1 mbar, 20 sccm N_2 gas flow, and filament temperature of 1650 °C.

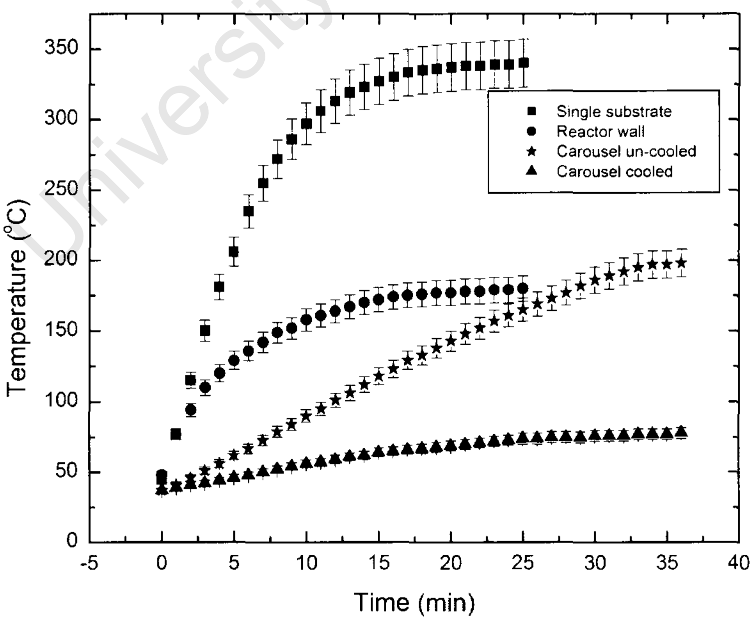

Figure 4.13: Rise in temperature of reactor components due to filament radiation

University of Cape Town

As indicated in Figure 4.13, each configuration reaches an equilibrium temperature in about 20 minutes, except for the case of the un-cooled carousel which stabilises after 35 minutes. As expected, the single substrate, 30 mm from filament, heats much faster, and reaches higher temperatures than the carousel, which can dissipate heat through the base plate. The cooled carousel arrives at a stable temperature between 60 °C and 70 °C within 10 minutes, and that temperature is maintained within ± 5°C. The data shows that the temperature of the reactor wall can exceed 150 °C after 10 min, which is at the limit of the recommended maximum operating temperature for Viton® O-rings [67]. Cooling the chamber with water, as described previously, is therefore necessary.

Effectiveness of the shutter

The effectiveness of the shutter was tested on a substrate, positioned in the carousel, and covered by the shutter. The system was operated for 8 minutes, with a filament temperature of 1650 °C, at 1 mbar, and 25 sccm of pure silane. On completion of this production cycle, the substrate was visually inspected for material deposit. No noticeable deposit was found on the substrate, indicating that the shutter is effective in controlling particle collection on the substrate.

Pressure range and flow rate

During system testing it was found to be difficult to set and maintain a flow rate lower than 10 sccm on the flow meters. The CD Calc software shows that the sensitivity of the flow meters does not double for a halving of the input pressure, and the flow meters will have to be used as calibrated in Table 4.1. This has the implication that the minimum flow rate for any gas will be 10 sccm. In a H_2:SiH_4 mixture of 90:10 the total flow rate will thus have to be at least 50 sccm and this will further, in conjunction with the vacuum pump limitations, determine the minimum pressure at which the system can be operated. Experimentally the minimum pressure achievable with 50 sccm flow rates is 3 mbar, and in the case of 100% silane at 10 sccm it is 0.3 mbar.

Filament ageing

Tungsten filament ageing is a major concern in thermal catalytic process, and it is associated with changing surface morphology, which leads to a decrease in filament

University of Cape Town

temperature, deteriorated electric properties of the filament, and later wire breakage [34]. The ageing of the filament can be ascribed to layers of Si-W alloys being formed on the surface and propagating to the centre, as well as tungsten evaporation, causing erosion and cracks [34]. In the system presented here, limitations in the vacuum pump and flow meter sensitivity have forced the experiments into a fairly high pressure regime of 3 to 30 mbar, where filament ageing is accelerated due to higher silane concentrations and interactions. As the filament ages in operation, its colour changes from bright yellow-white to a darker orange, indicating a cooler temperature, while the current and voltage indicate that the electrical power is unchanged.

Figure 4.14, shows a heated filament during operation. The difference between the hot region (c) and the cracked cooler region (b) is apparent.

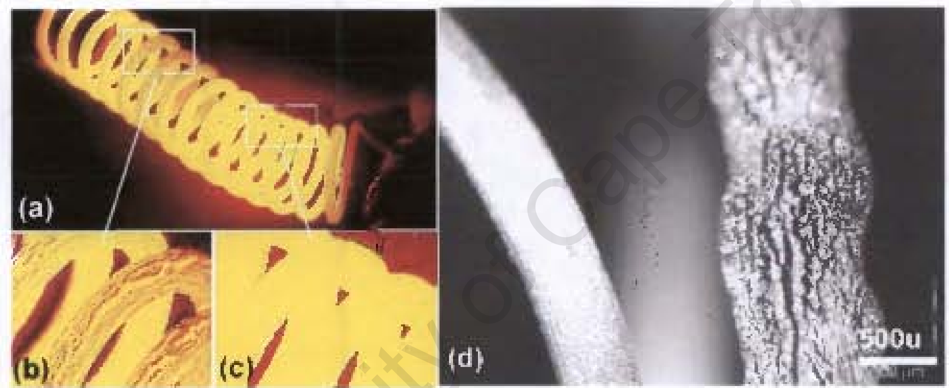

Figure 4.14: Tungsten filament degradation. (a) Operational filament, with (b) cooler cracked section, (c) hot less degraded section and (d) optically enlarged cold section

University of Cape Town

Figure 4.14(d) shows an optically enlarged section of the same filament, after it had operated at 1700°C and 25 sccm silane at a pressure of 1 mbar. It had failed after 28 min operation. Similar results have been reported [68], in which scanning electron microscopy of aged wires revealed a surface both rougher and more irregular than new or heat-treated wires. The morphology is thought to be characteristic of Si deposition, either as free Si or as a silicide.

Temperature measurement errors

During the first experiments, it was found, that the pyrometer temperature measurement does not always correlate with the data, as given in Figure 4.12, and is consistently lower in most cases. In a brief investigation, three likely sources of error were found:

A. Change in transmittance of the window;

B. Positioning of the pyrometer measurement area;

C. Emissivity of the filament.

Details and findings of each are discussed in more detail below.

A. Change in transmittance of the window

During the first particle production experiments, it was noticed that the window is subjected to the Si nanoparticle deposition. At high pressures of 6 to 24 mbar this can happen rapidly. To measure the effect on the pyrometer temperature readings, an experiment was performed, where the pyrometer is mounted as indicated in Figure 4.11, and directed at the same location on the filament. In a series of measurements, in 2 minute intervals, the temperature was measured. The pressure is maintained at 1 mbar of 25 sccm silane, and the current of the starting temperature of 1650 °C maintained for the duration of the experiment. Figure 4.15 clearly shows an apparent 100 °C drop in measured temperature over 10 min.

University of Cape Town

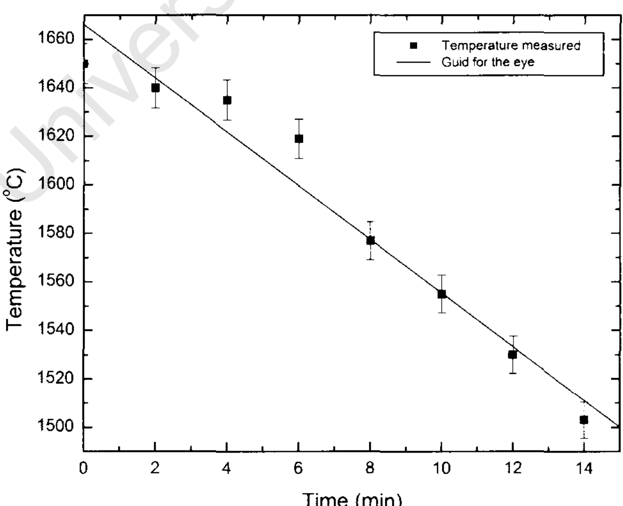

Figure 4.15: Effect of glass fogging on filament temperature measurements with pyrometer

Although the effect of the ageing of the filament could not be taken into consideration, the visibly yellow to orange deposit on the glass indicates that a large portion of the measurement error can be ascribed to the loss in transmission due to particle deposits on the glass. Following this experiment, the shutter is so mounted that, in its open position, it covers the view port and prevents deposits on the window.

B. Positioning of the measurement area

A further effect noticed during temperature measurements, was the change in temperature reading with a slight movement of the pyrometer, which has an optically inserted circle in the centre of the view finder. To test the effect of a misplaced circle, a filament with 1, 2 and 3 full windings was constructed and mounted in the reaction chamber. Figure 4.16 has been photographed through the view finder of the pyrometer and shows the overlay circle as well as the different winding sections. The filament temperature was maintained at 1650 °C, and the gas pressure at 0.3 mbar of N_2. Using the same configuration as used for the filament current calibration as seen in Figure 4.11, four temperature readings of each section (1, 2 and 3 windings) of the filament were taken and plotted. Since the current for all windings is the same, it can be assumed that the temperature should be the same. The mean value of the temperature measurements for each section are plotted in Figure 4.17, and show that a measurement error of more than 220 °C can be introduced by the positioning of the pyrometer.

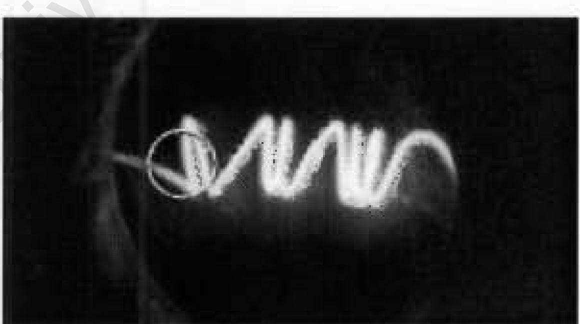

Figure 4.16: Filament with separated 1,2 and 3 turns as seen through pyrometer

For accurate comparative temperature readings, using the only available pyrometer, it is thus imperative to keep the pyrometer pointed at the same location on the filament, and to fabricate filaments consistently in all respects.

University of Cape Town

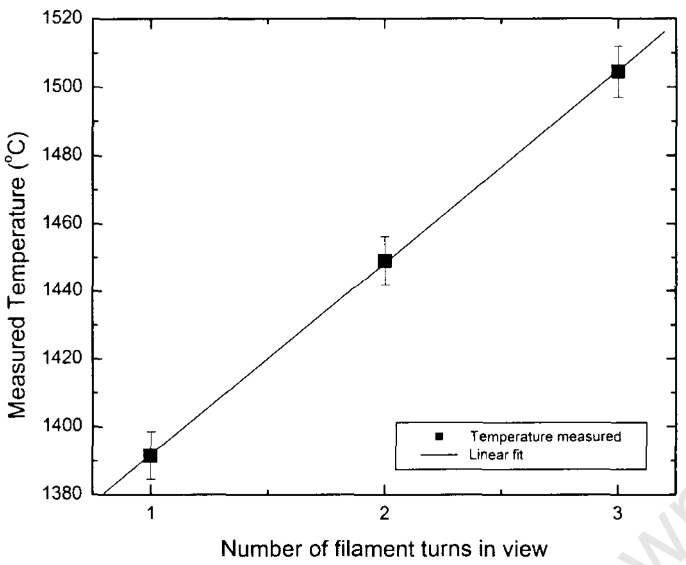

Figure 4.17: Error due to pyrometer measurement area position

C. Emissivity of the filament

The emissivity of the filament is an important parameter in the calibration of any optical instrument used for its temperature measurement. The pyrometer used has an emissivity adjustment, to compensate for the material measured. For elemental tungsten the emissivity is commonly given as 0.44 [69]. As reported before, the properties of the filament material however change during deposition, by the formation of a new material, possibly with a different emissivity. If the single wavelength pyrometer is used to measure the temperature of this changed filament, using the same emissivity setting, the measurement will have an error. This emissivity change has been known and reported in the literature [34], but is very difficult to compensate for. In fact, the change in emissivity is ignored, and instead the filament voltage or current are kept constant to maintain the desired temperature.

Now that the TCP system has been assembled and tested, a series of experiments can be conducted, to determine what material will be produced, for a variation in the parameters of the system.

University of Cape Town

5. SILICON NANOPARTICLE PRODUCTION AND CHARACTERISATION

The aim of the research is to synthesise silicon nanoparticles using a thermal catalytic pyrolysis system. In the previous chapter, the design and assembly of such a system, as well as its performance, was discussed. The system was found to perform reasonably well, and to be ready for synthesis experiments. In this chapter, the process and the production, of silicon material will be described. Furthermore, the characterisation techniques required to investigate the characteristics of the as-produced material will be discussed.

The overall experimental process, leading to material production and characterisation, can best be described with the help of the flow diagram in Figure 5.1. In the description, letters given in brackets refer to the process step and corresponding letter in Figure 5.1. Arrows in the diagram indicate the process flow direction. Starting in the top left corner: (a) all substrates were sonicated in acetone for 1 hour, after which they were air dried, and wiped with a clean cotton cloth. Next, each substrate was weighed (b), and the measurements were recorded (c). The substrates were again cleaned, as described above (d), and were stored in the clean substrate holder (Figure 5.2), ready for production. The production process (e) was now performed, as described in detail later in this chapter. Upon completion of the production process, substrates were stored in the substrate holder and the production process repeated with different parameters. After all experiments were completed, all substrates were weighed again (f), and the data recorded (g). The mass of the material deposited on the substrate was now calculated, by subtracting the weight of the "clean" substrates from that measured on the same substrate after deposition (h).

University of Cape Town

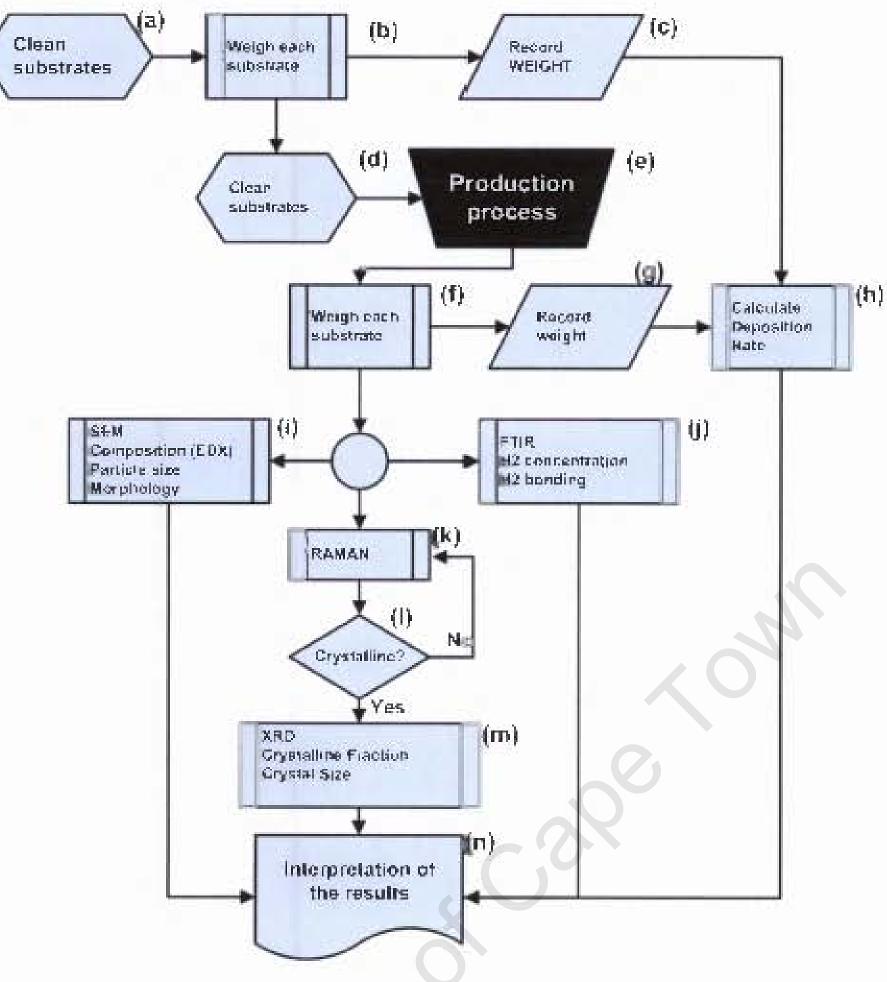

Figure 5.1: Overall experimental process, flow diagram

For SEM imaging (i), a small portion of the material, deposited on the substrate, was transferred directly to a carbon sticker, and subjected to a carbon sputter coating, for 5 seconds. Similarly, only a small portion of the material was used for FTIR spectroscopy (j), which process is described in more detail later in this chapter. Raman spectra (n), were initially collected directly from the substrate, or from material deposited on a microscope slide. Samples that showed a sign of crystalline fraction, in the Raman spectra, were taken to X-ray powder diffraction (XRD) (p). At the end of the experimental process, all information was collated, correlated and the results interpreted.

University of Cape Town

Figure 5.2: Substrate holder, loaded with substrates, covered with as-deposited material.
(Scratch marks resulted from FTIR material collection)

5.1 Powder production

The process leading to silicon material production, will now be discussed in more detail, starting with the choice of the parameter space. In all experiments, silane (SiH_4) was used as the silicon precursor. In this research, the choice of parameters was influenced by the capabilities of the thermal catalytic pyrolysis system. In chapter 3, parameters, borrowed from the HWCVD processes, were suggested as a guideline for the construction of this system, but, due to limited components, could not be fully implemented. Two of these limitations, reported in section 4.5, affect the choice of the parameter space, namely the minimum controllable flow rate of 10 sccm, for hydrogen and silane, as well as the lowest achievable operating pressure of 3 mbar.

University of Cape Town

Taking these limitations into account, the parameter matrix, as given in Table 5.5, is designed for the experiments. Numbers in the non-shaded area represent the sample numbers, and, at the same time, correspond to the number registered on the substrate. Experiments were conducted in 5 series, with the hydrogen dilution being fixed for each series, at the percentage indicated in Table 5.5. The pressure was varied, as indicated in the column of the table. As an example, sample 32 was produced on the substrate marked 32, at 6 mbar with a hydrogen dilution of 40%.

		Operating pressure (mbar)				
		3	**6**	**12**	**24**	**48**
Hydrogen dilution ($\%H_2$)	**80% (Series 1)**	11	12	13	14	15
	60% (Series 2)	21	22	23	24	25
	40% (Series 3)	31	32	33	34	35
	20% (Series 4)	41	42	43	44	45
	0% (Series 5) (100% SiH_4)	51	52	53	54	55

Table 5.1: Experimental parameter matrix

All other parameters, including the filament temperature, substrate temperature and total flow rate were kept constant for all experiments. As the aim of the research is nanoparticle (powder) production, the substrates are cooled, to suit the conditions for particle formation, as mentioned in chapter 3. All fixed parameters are given below:

Total flow rate (H_2 and SiH_4)	50 sccm
Filament temperature: (T_{Fil})	1650 °C ± 50 °C
Substrate temperature: (T_{Sub})	60 °C ± 5 °C
Deposition time per sample	8 min
Settling time between depositions	1 min
Cooling water flow rate	± 2 $litre.min^{-1}$

Using the full set of variable and fixed parameters discussed above, the system was then used, to produce powders. The details of the production process will be described with the help of Figure 5.3. In the following description, letters given in brackets, refer to the process step and corresponding letter in the same figure. Arrows in the diagram indicate the process flow.

University of Cape Town

Starting in the top left corner; (a) Remove the filament holder from the chamber, and replace the tungsten filament. (b) Load 6 substrates into the carousel, with numbers corresponding to the carousel section, and mount the aperture plate on top of the carousel. Upon completion, substrate 1 must be positioned in the aperture. (c) Close the reaction chamber (reactor) and make sure that all ports are closed, and the gas supply pipe is in place. Three G-clamps should hold the two halves of the reactor in place. (d) Open the pressure regulator valve (below reactor) and (e) start the vacuum pump. Once the vacuum has reached a base pressure of 0.1 mbar, purge the chamber twice with nitrogen (f), by opening the stop valve, and nitrogen valve on the gas control panel. The nitrogen flow can be set at 100 sccm. After the second purging of the reactor, leave the vacuum pump running until a base pressure of 0.01 mbar is reached. (g) Close the shutter, and switch on the power supply. (h) Adjust the filament current to the corresponding temperature, consulting the current vs. temperature data (Figure 4.12). (i) Allow the temperature of all components in the system to settle, and correct the filament temperature (current), before continuing. (j)The precursor gas can now be introduced. Allow 4 minutes for the system to settle, and use that time to manually adjust the flow rate and pressure (k). Now, before starting the production, correct the filament temperature again (l) and, correct the pressure with regulator valve (m). Once in order, open the shutter (n) and start the timer (o). While the timer is running (p), monitor the flow rate, filament temperature and pressure until the timer runs out (q). Close the shutter (s), reset the timer (r) and rotate the carousel to position the next substrate in the aperture (t). Using the parameters of the next experiment (u), repeat the process, starting again at setting the parameters (k). Directly following the completion of the last experiment (v), close the shutter (w), close the silane and hydrogen supply (x), and flush the system with nitrogen for 4 minutes (y). The reactor can now be opened, and the substrates can be removed and stored.

University of Cape Town

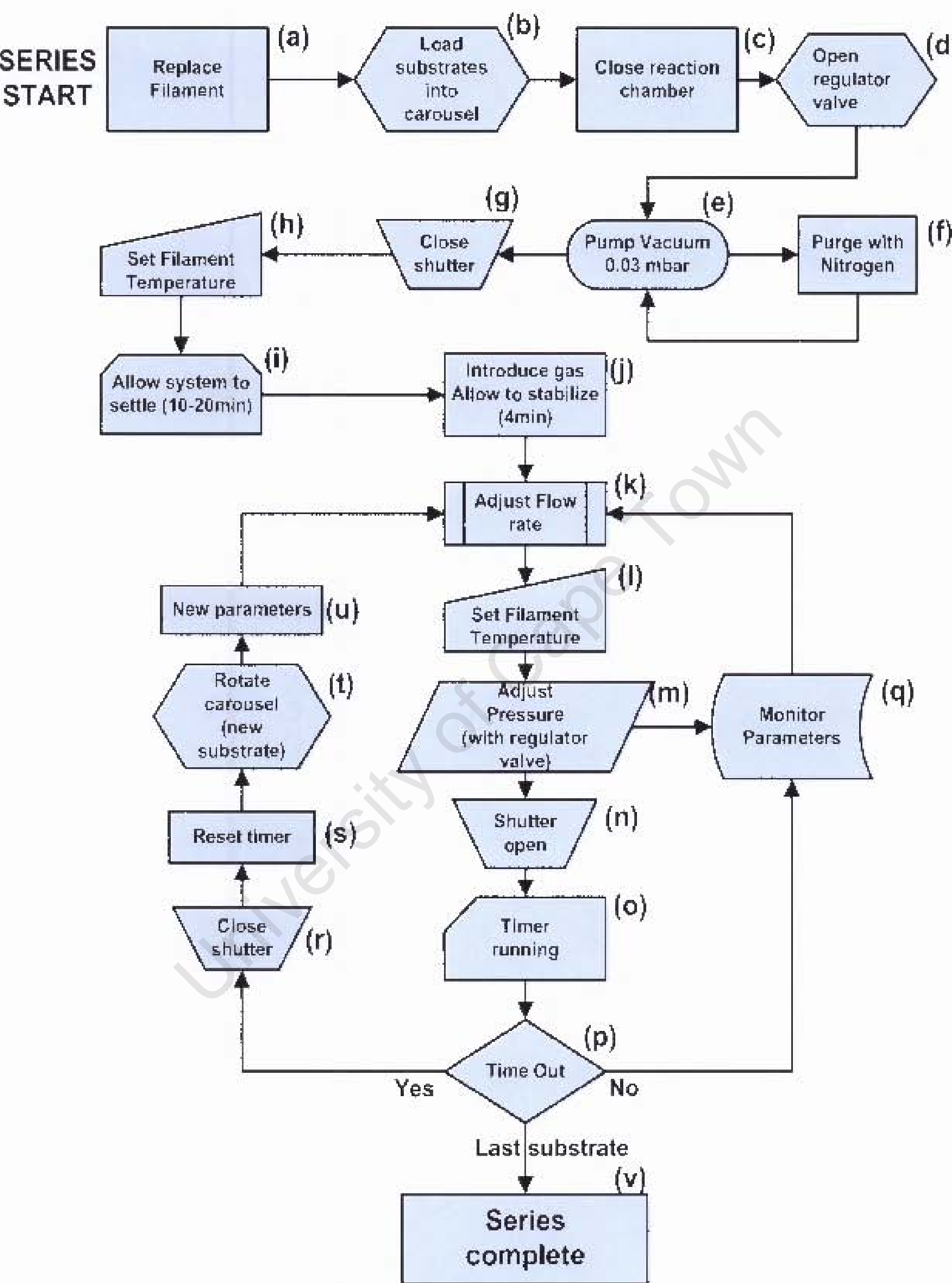

University of Cape Town

Figure 5.3: Powder production process flow diagram

Using the parameters as given in Table 5.1 each series of experiments, comprising the 5 substrates loaded, was conducted, with a fixed hydrogen dilution ratio corresponding to the chosen value for that series, while the pressure was varied, starting at the lower level (3 mbar) and progressing to 48 mbar, with the last substrate. Upon completion of a series, all material in the chamber was collected for possible investigation and characterisation.

Figure 5.4 gives an indication of the different locations, inside the chamber, where material was collected.

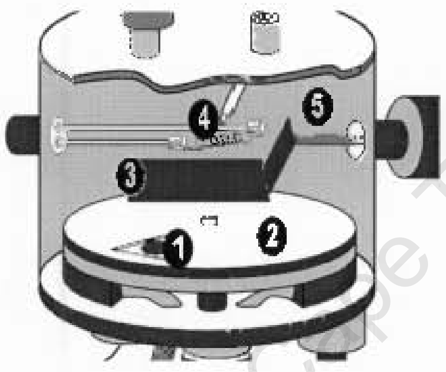

Figure 5.4: Locations in the reactor where material was collected

The stainless steel substrates (1) were always stored in the substrate holder, while material on the aperture plate (2), shutter plate (3), filament holder rod, and gas inlet pipe (4), and on the reactor wall (5) was wiped off with a small silicon rubber 'spatula' and stored in marked glass sample bottles. Apart from the substrates, only material that looked markedly different in colour (dark brown) from that produced in the series, was considered for characterisation.

5.2 Characterisation techniques

The aim of the research is the production of silicon nanoparticles, through thermal catalytic pyrolysis. The as-produced material therefore has to be characterised, to verify that the research goal has been achieved.

Starting at the macroscopic level, the position, quantity, and colour of the material can be visually observed and photographed. The material can be touched, scraped or wiped,

University of Cape Town

to reveal its macrostructure. Furthermore, the production rate can be determined by the weight of material, deposited on a known surface area. For a better understanding of the microstructure of the material, an optical microscope can be used. However, to determine the presence of nanoparticles, a scanning electron microscope (SEM), able to resolve 5nm, is essential. EDX, a part of most SEM's, can furthermore be used to determine the elemental composition of the material, which is important information to verify what has been produced. FTIR spectroscopy can also supply information on particle composition, and notably, the absorption spectrum will show Si-O and Si-H bonds, both important for HWCVD produced silicon.

Finally, to determine the crystalline order in the material produced, X-ray diffraction can be employed to give an indication of order (crystallinity) and crystal orientation, while RAMAN spectroscopy can show order and crystalline fraction. A brief summary of the characterisation techniques is given in Table 5.2 below.

	Technique	**Character revealed**
Morphological Investigation **(Macro - and Microscopic)**	Visual inspection (optical photo)	Colour, macro structure, soft/hard, loose/dense etc.
	Sensitive Balance	Deposition rate Density (if volume is known)
	Optical microscopy (optical photo)	Micro-structure, smooth/rough, even deposit/cauliflower structure etc.
	SEM (scanning electron microscopy)	Size, shape, aggregation, agglomeration, surface roughness, microstructure
Composition analysis	EDX (energy dispersive x-ray spectroscopy	Elemental composition. Indication of ratios.
	FTIR (Fourier transform infrared spectroscopy)	Bonding structure and elemental composition.
Micro-structural Investigation	XRD (x-ray powder diffraction)	Indication of order and crystalline orientation
	RAMAN Spectroscopy	Indication of order and crystalline fraction

Table 5.2: Summary of characterisation techniques suitable, and available, for silicon material characterisation

University of Cape Town

These are important techniques for silicon material characterisation in general, and for the characterisation of silicon nanoparticles. Each technique will now be discussed in more detail.

Macroscopic investigation

Macroscopic investigations were typically started with a visual observation of the material produced. This information was captured on a digital camera, for later reference to the position and colour of the material deposited. Furthermore, the material was wiped and blown onto, to determine its adhesion to the surface, and to be able to describe it as either a powder or coating.

The quantitative yield of material, deposited as thin films, is usually expressed as a function of thickness and time (e.g. Å/sec). If the material produced in this research is, however, a powder or porous layer, this technique will not be applicable. The ratio of the weight of the material to the substrate area and synthesis time was used to define the synthesis rate in $\mu g.mm^{-2}min^{-1}$. This unit offers a way of comparing sample yields under different production conditions. The weight of each substrate was measured before and after synthesis, and the area of each substrate was also determined. The substrate areas were calculated by scanning them, using a conventional computer scanner, at 600 dpi, and processing the image with ImageJ V1.16b software. This was calibrated at a linear resolution of 28 mm = 132 pixels, with a pixel aspect ratio of 1. In these studies, the weight was determined using a Mettler AX 205 with an accuracy of 10 µg. During deposition, the total time of the synthesis per substrate was recorded.

University of Cape Town

Microscopic characterisation

In microscopic investigations, the aim is to determine the morphology of the material at the microscopic level. It is important to determine if the material is in the form of a layer, a porous structure or powder. Furthermore, if the material is a powder, it is important to determine the primary particle size and shape, as well as the level of agglomeration and aggregation of the particles. The main microscopic characterisation technique used, for material produced in this research, was the scanning electron microscope (SEM). A SEM forms a microscopic image by using electrons, emitted from an electron source. These electrons are focused through electromagnetic lenses onto the sample. As the electron beam is scanned across the sample, interactions between the

electron and the sample, create secondary electrons, which are detected by an electron detector. Using the raster of the scan, as well as the intensity of the detector output, a microscopic image of the sample is formed. For this research, a LEO 1525 SEM was used, at 5 and 10 kV settings with an aperture of 10 μ. The InLens was used, and the pressure of the system and gun were normally in the order of 10^{-7} mbar and 10^{-10} mbar respectively.

Composition analysis

The main techniques used to determination the composition of the material produced are SEM/EDX and FTIR. Energy Dispersive X-ray Spectroscopy (EDX) makes use of the electron beam of the SEM to construct an x-ray fluorescence spectrum. This technique offers an easy and fast elemental analysis of the sample in areas as small as 5*nm* in diameter. The result should, however, be seen as an indicative, and not absolute analysis. The technique was used to determine the composition of the nanoparticles during SEM imaging under the conditions described above.

Fourier transform infrared spectroscopy (FTIR) is an important tool in the chemical analysis of a variety of substances, including gases, liquids and solids. It is widely used, both in research and industry, for measurement and quality control. The technique has also been used extensively to characterise silicon films [33,47,51,70], and recently silicon nanoparticles [5,31,71]. Using FTIR, it is possible to obtain information about the surface properties of a material, such as the coverage and bonding of hydrogen and/or oxygen, and the stoichiometry of the surface oxide layer. The basic principle of FTIR is based on the absorption of infrared (IR) radiation, corresponding to rotational and vibrational states of bound atoms. Where resonance takes place, energy will be absorbed. These molecular vibrations give rise to absorption bands in the infrared region of the spectrum. The frequency, or wave number, of the vibrations can be associated with a particular bond type, and each material will have its characteristic absorption spectrum (fingerprint) that relates to its composition [72]. For silicon the bands, corresponding to the bond types, are given in Table 5.5 below. Bands at 640, 840 and 880 cm^{-1} can be assigned to the Si-H and SiH_2 rocking, bending and scissoring mode vibrations, while the bands between 2000 and 2100 cm^{-1} arise from Si-H, SiH_2 and $(SiH2)_n$ stretching vibrations. The Si-H, SiH_2 and (SiH_2)n stretching modes are

University of Cape Town

usually observed in highly porous a-Si:H films [71]. In silicon nanopowders, $(SiH_2)_n$ stretching can therefore be expected at 2100 cm^{-1}. A Si-O absorption mode should be found at about 1070 cm^{-1}, and O-H bending at 1630 cm^{-1}. Si-O-Si and O-Si-O wagging modes should appear at 2250 cm^{-1} and 460 cm^{-1} respectively [71]. Figure 5.3 offers a summary of the absorption peaks for silicon. To perform the FTIR measurements, Si powder (less than 1mg) was mixed with 100 mg of KBr (potassium bromide), which was previously dried for 8 hours at 120 °C in an oven. The mixture was ground together in a marble mortar, and formed a powder of uniform colour. This powder was pressed with a 10 ton force, for 5 minutes, under a vacuum of about 1mbar, into a semi-transparent disk of 12 mm diameter and a thickness of 0.25 - 0.5 mm. One blank KBr disk was also pressed to serve as a reference. A Nicolette – Nexus 470 FT-IR spectrometer was used to capture the absorption spectra of the samples. The IR spectra of the KBr reference disk was recorded first, and used to compensate for absorption in the KBr and atmosphere. Using the instrument in transmission mode, the spectra were recorded in the 400 - 4000 cm^{-1} range, in steps of 2 cm^{-1}.

Wave number (cm^{-1})	Stretching	Scissoring/Bending	Rocking	Wagging	**What the band indicates:**
460			O-Si-O		Surface oxidisation
630-640		Si-H, SiH_2	Si-H, SiH_2, SiH_3, $(SiH_2)_n$		
840		SiH_2, $(SiH_2)_n$			
880		Si-H, SiH_2			Surface-bound hydrogen
942		O-H, Si-OH			Surface-bound hydroxyl groups
1070	Si-O				Partial surface oxidisation
1630		O-H, Si-OH	Si-O-Si		Surface-bound hydroxyl groups
2000 - 2050	Si-H				Surface-bound hydrogen
2070 - 2100*	SiH_2, $(SiH_2)_n$				In thin films - highly porous or indicate particles. (large void fraction)
2142*	Si-H				Particles partially covered by hydrogen
2250*			Si-O-Si		Surface bound oxygen
Data in this table collated from: [71],[31], [73]					

Table 5.3: a-Si:H infrared absorption peaks and indication of cause

University of Cape Town

Microstructural characterisation

XRD and Raman spectroscopy were the main techniques, used for microstructural characterisation of the material produced. While XRD was used to check the crystal structure and phase composition of the material, i.e. Si or SiO_2, Raman spectroscopy was mainly used to determine the crystalline fraction of the material.

X-ray diffraction (XRD) is a powerful technique that is used to identify the phases and crystal orientation in crystalline materials. Each type of material generates a unique diffraction pattern, which can be matched against the database [74] of experimental or calculated patterns of a reference material.
XRD is based on Bragg's law, which results in a simple equation:

$$n\lambda = 2d\sin\theta, \qquad (5.1)$$

relating the x-ray wavelength λ and the diffraction angle θ, with the inter-planar spacing d, where n is an integer. This equation is simply the interference condition for radiation diffraction by a set of uniformly spaced atomic planes, and n can be seen as the order of diffraction.
Silicon is a four-fold coordinated atom that is normally tetrahedrally bonded to four neighbouring atoms, which in crystalline silicon forms a well-ordered diamond cubic structure.
Figure 5.5 shows the arrangement of the silicon atoms in a unit cell, with the numbers, in indicating the height of the atom above the base of the cube as a fraction of the cell dimension.

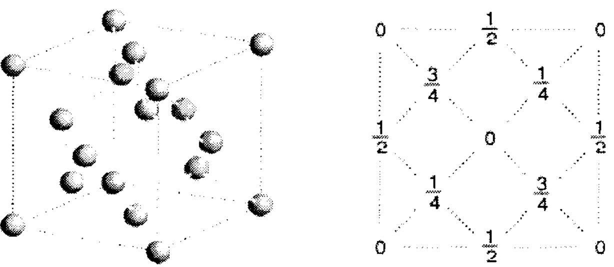

Figure 5.5: (a) Crystal structure of silicon. (b) Atomic position of the cubic cell of the diamond structure projected on a cube face [75]

University of Cape Town

Lattice planes, and lattice directions of the crystal, can be described by a mathematical description known as Miller indices. This allows the specification, investigation, and discussion of specific planes and directions of a crystal, as shown below.

For silicon, the first three expected diffraction peaks, corresponding to the set of lattice planes given by the Miller indices, (111), (220) and (311) are shown in Table 5.4 below.

Diffraction angle for CuK_α radiation (2θ)	**Silicon orientation**
28.5°	(111)
47°	(220)
56°	(311)

Table 5.4: Silicon diffraction peaks for CuK_α radiation [76].

The orientation of these planes in the cubic unit cell is graphically illustrated in Figure 5.6.

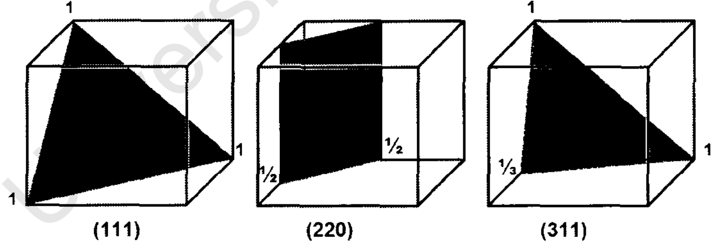

Figure 5.6: Millers indices identify crystal planes in Si.

In amorphous silicon the atoms form a continuous random network (no long range order is present), and so sharp diffraction peaks are not expected.

For XRD characterisation of the as-produced material, the powder was ground in an agate mortar, prior to being sprinkle loaded onto a single crystal of Si coated with Vaseline. The commercially acquired silicon wafer was cut to specific angle, to avoid

University of Cape Town

any contribution to the diffraction pattern. The X-ray powder diffractometer used, was a Phillips PW 1830, operating at 45 kV and 40mA. Copper K_α radiation with a wavelength of 1.5406 Å was used. The diffraction pattern was recorded from 5° to 90° in 2θ, with a step size of 0.02°, and 1 second step time.

Raman spectroscopy is well suited to detecting crystalline phases in amorphous material, e.g. a-Si:H, and may be used to calculate the crystalline fraction [77]. Raman scattering is very sensitive to small changes in the short-range order, and usually has the advantage of being non destructive. Raman scattering describes the energy loss and change in wavelength of monochromatic light after interacting with atoms in the material [72]. The lost energy vibrates inter-atomic bonds and rotates atoms about their bonds. Each atomic bond vibration, or bond rotation, causes a unique energy loss and subsequent shift in wavelength of the original beam (Raman shift). Measuring the spectrum of wavelength shifts allows the identification of molecular species on the sample surface, or inside a transparent sample.

In general, the Raman spectrum of silicon will have a sharp peak at 520 cm^{-1} if crystalline, while amorphous silicon will have a broad peak at around 480 cm^{-1} [49]. The relative areas of these two (de-convoluted) peaks can be used to calculate the crystalline fraction of the material [77]. A shift towards lower wave number and a decrease in peak intensity has been observed, as the particle size decreases [32]. The features at specific Raman shifts, and corresponding material properties, in general, for silicon are summarised in Table 5.5.

Raman shift (cm^{-1})	Feature	Material properties
480	Broad peak	Amorphous silicon (disorder)
500	Medium peak	Grain boundaries or micro grains.
430-530	Broad structure	Nano particulate (powder)
514 -522	Narrow peak	Crystalline nanoparticles
520	Sharp, narrow peak	Crystalline silicon
Data in this table collated from: [32,59,77,78]		

Table 5.5: Summary of features and properties at specific Raman shifts for silicon

University of Cape Town

For Raman spectroscopy, the silicon samples produced were placed on a glass microscope slide, or left on the stainless steel substrate, depending upon the layer thickness. For the collection of Raman spectra, a Dilor XY dispersive laser Raman spectrometer, with a CCD detector, was used in combination with an Olympus optical microscope, using a 50x objective lens. Two lasers were used, the first being a Coherent Innova 300 Argon laser (green line at 514.5 nm, and beam intensity of 100 mW at source), and a Spectra-Physics Stabilite 2017 Krypton laser (yellow-green line at 568.2 nm, and a beam intensity of 100 mW at source).

University of Cape Town

6. RESULTS AND DISCUSSION

The thermal catalytic pyrolysis system, as described in chapter 4, was used to produce silicon material, using the production process described in chapter 5. As illustrated below, nanopowders were produced under change of pressure and hydrogen concentration. The filament and substrate temperatures as well as the flow rate and production time were fixed for all samples produced. This chapter describes the material produced, yield and characterisation, using the techniques described before. For some of the techniques, a commercial silicon nanopowder was used for comparison, and will be referred to as intrinsic silicon (i-Si). According to the manufacturer [79], the powder is synthesised by laser pyrolysis, resulting in crystalline nanoparticles. Particle diameters smaller than 100 nm and a specific surface area larger than 80 m^2g^{-1}, are specified.
In the following characterisation discussion, reference will be made to the sample number, operating pressure and hydrogen dilution, as indicated in the parameter matrix (Table 5.1). As discussed in the previous chapter, samples were produced with 0, 20, 40, 60 and 80% hydrogen dilution, and a total constant flow rate of 50 sccm, at 3, 6, 12, 24 and 48 mbar. The filament temperature was maintained at 1650 °C and no substrate exceed 70°C. For each series, 5 substrates where loaded into the carousel, and single filament was used, for the production of all 5 samples of the series.

University of Cape Town

6.1 General appearance and yield of the Si produced

Upon completion of the synthesis process, on a series of substrates, the reaction chamber is opened and visually inspected. As can be seen in Figure 6.1(a) and (b), a powdery substance is deposited on all surfaces inside the reaction chamber. The as-prepared powder, shown on the aperture plate in Figure 6.1(a), varies in colour from yellowish to dark brown. The material is a powder-like substance and can be collected without effort. In Figure 6.1(c), this is demonstrated with a steel ruler, but a silicon

rubber spatula was mostly used for collecting the material. In many samples, the material deposited can be blown off the surface, indicating how loosely the material is deposited. Material deposited in some areas i.e. on the gas inlet pipe, shutter and filament holder (visible in Figure 6.1 (b)), often has a much darker brown colour compared to material deposited on the substrates. As mentioned in chapter 5, some of this material was collected for possible investigation.

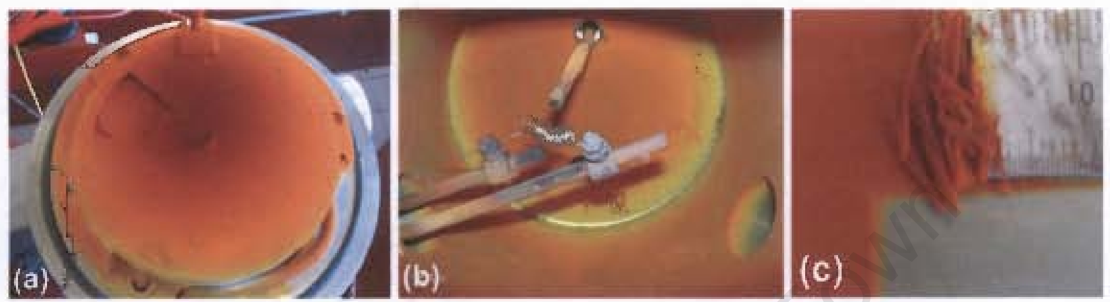

Figure 6.1: Material produced, (a) deposits on aperture plate; (b) inside chamber; and (c) flaking when scraped off

Material shown in Figure 6.1 is the end-result of the completed series 5, produced at 100% silane, with progressive steps in pressure, and a total deposition time of 40 min. All other series produced similar results, typically with less material as hydrogen dilutions increased. In Figure 6.1(a), one substrate, positioned in the carousel, is clearly visible though the aperture of the aperture plate.

The process, of determining the yield was described in chapter 5. The weight of material, deposited on each substrate, is expressed as a ratio to the surface area and production time. Figure 6.2 shows the results of this calculation against the pressure variation. The figure represents all samples from series indicated in the parameter matrix given in Table 5.1.

University of Cape Town

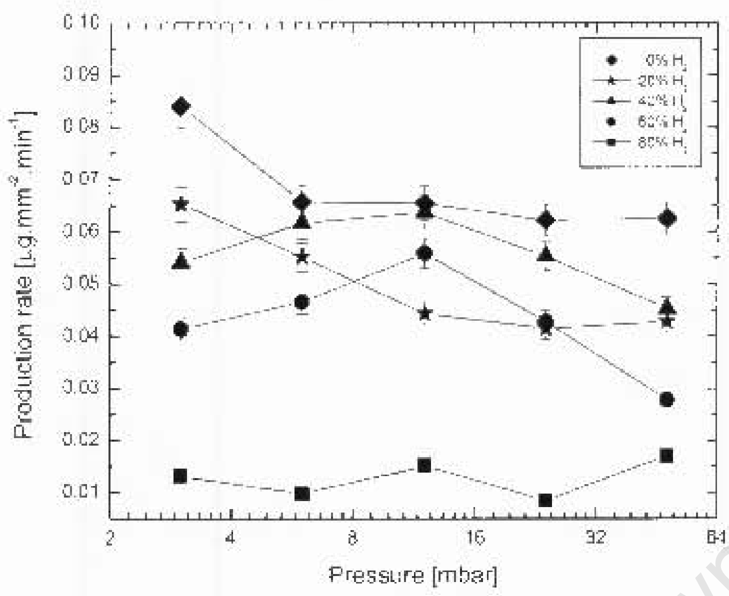

Figure 6.2: Production rates at varying hydrogen dilutions and pressures

As can be expected, Figure 6.2 shows how, in general, the production rate increases with decrease in hydrogen dilution, up to the maximum of 100% silane. The general decrease in production rate towards higher pressures is unexpected, and should rather increase [48]. This effect can possibly be ascribed to the ageing of the filament, which, for the samples taken at the lower pressure, was still very new. In the ageing process the properties, and thus the catalytic and pyrolitic activity, of the filament will change, affecting the production rate. This decrease of deposition rate with filament 'on-time', due to filament ageing has been reported by Wang [34].

6.2 Microstructure and morphology

All characterisation of microstructure and morphology, of the deposited powder, was performed with SEM as described in chapter 5. Materials investigated with SEM, are the samples numbered: 11, 21, 31, 33, 35, 41, 44, 51 and 52. Starting with the undisturbed surface of sample 35 (Figure 6.3), produced at 48 mbar and 40% H_2, the morphology of the as-deposited material was investigated.

Figure 6.3 (a) and (b) are the same sample at different magnifications.

University of Cape Town

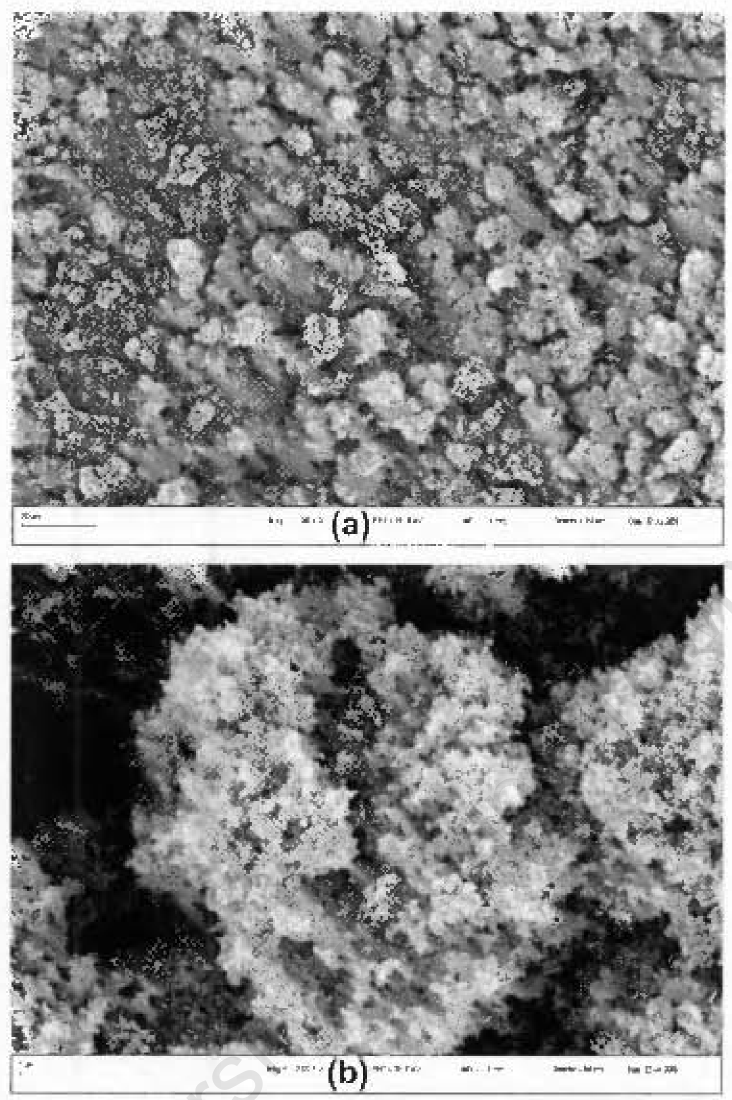

Figure 6.3: Sample 35, as-deposited on the substrate at low (a) and high (b) magnification

Figure 6.3(a) reveals a porous microstructure, with, what looks like, clusters of uneven micron sized particles or clusters. A further magnification of one of these clusters (Figure 6.3(b)) reveals a highly porous agglomeration of nanoparticles, the size of which is difficult to ascertain. A further magnification of the same cluster (Figure 6.4) clearly shows agglomerated nanoparticles, with a diameter roughly estimated at 40 nm.

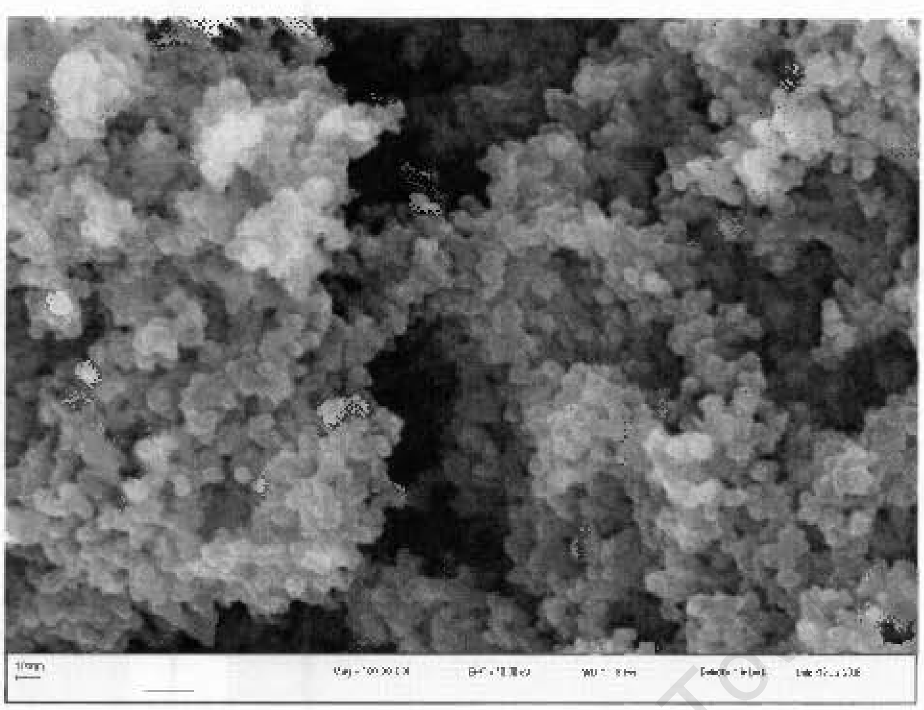

Figure 6.4: Particle size and agglomeration of sample 35

The high level of porosity in the nanopowder deposit is evident in Figure 6.4. A large amount of voids can be seen between the clusters of agglomerated nanoparticles. The material can best be described as a highly porous agglomeration of silicon nanoparticles.

While all samples, investigated with SEM, reveal the presence of nanoparticles, the level of aggregation varies, not only with a change in pressure or hydrogen dilution, but also surprisingly, within the same sample. Examples are given below.

University of Cape Town

Sample 11, produced at 3 mbar and 80% dilution (Figure 6.5), shows a high level of agglomeration and aggregation, with indications, that the primary particles, are in the process of forming porous layers. Agglomerates and aggregates are in the micron size range.

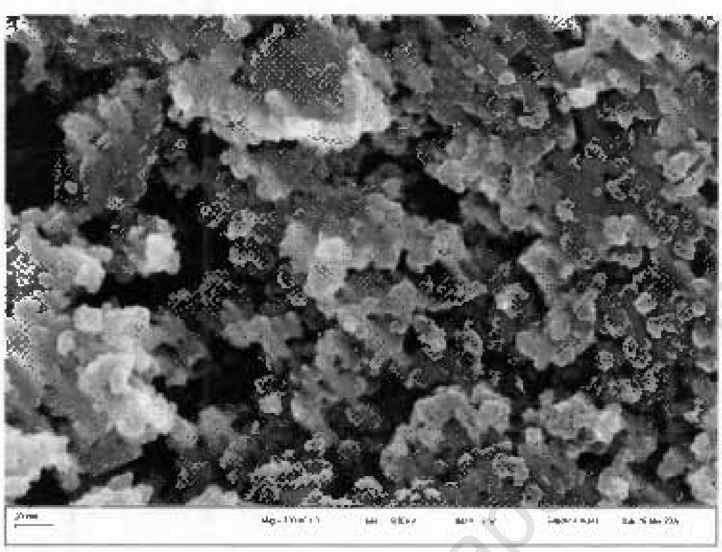

Figure 6.5: Sample 11 produced at 3mbar and 80% H_2

In sample 31 (Figure 6.6), produced at 3 mbar and 40% dilution, clearly identifiable agglomerated nanoparticles are visible. Judging by the scale bar of the SEM micrograph, the particle size is in the order of 50-80 nm with a fair size distribution.

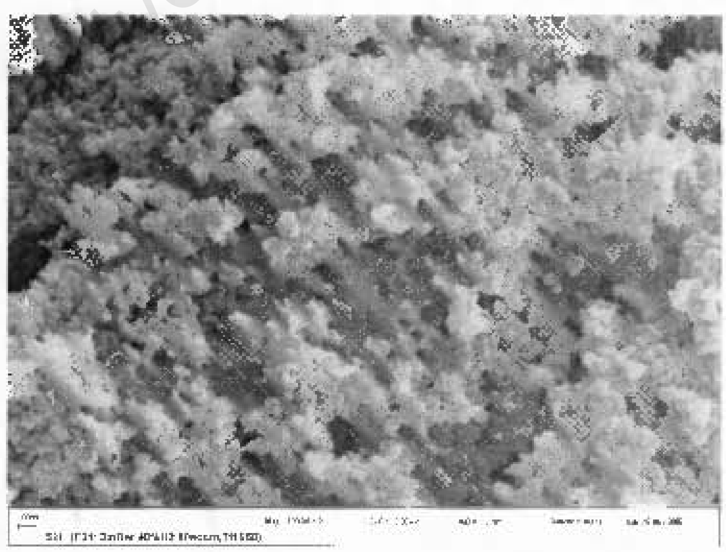

Figure 6.6: Sample 31 produced at 3mbar and 40% H_2

Sample 51 (Figure 6.7), produced at 3 mbar and 100% silane, displays very similar characteristics to those of sample 31 discussed above.

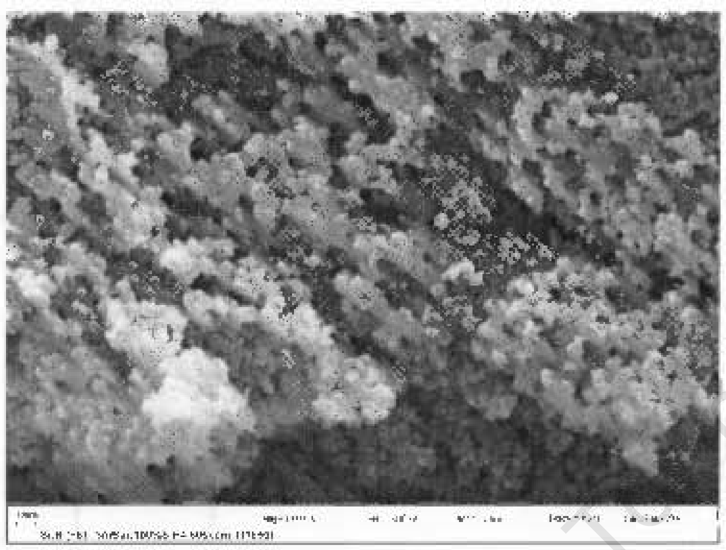

Figure 6.7: Sample 51 produced at 3mbar and 0% H_2 (pure silane)

From the comparison above, it is thus difficult to determine a trend in the influence of hydrogen dilution on particle size. To complicate matters further, the morphology, within the sample, is found to change, depending upon which part of the sample is investigated. An example is given in Figure 6.8, which is a micrograph of the same sample 51, depicted in (Figure 6.7).

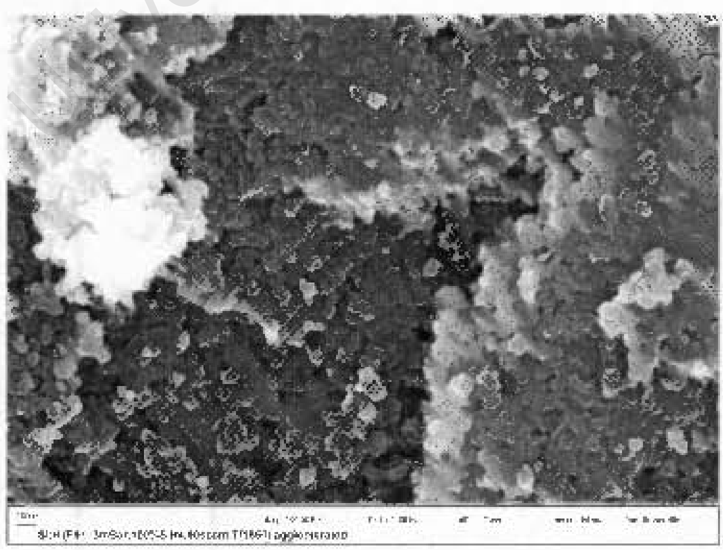

Figure 6.8: Sample 51 at a different position to Figure 6.7

University of Cape Town

Completely different in nature to the particles in Figure 6.7, the particles in Figure 6.8 are highly aggregated. Similar occurrences have been found in almost all samples investigated on SEM stickers. The cause of the discrepancy might arise from the fact that particles and aggregates form, and deposit onto the substrate, in porous layers. During transfer of the material to the SEM sticker, these layers are disturbed and revealed on the surface. The loose particles in the top left corner of Figure 6.8 may offer support to this argument. Furthermore, the difference in morphology, of the material produced, in the same sample, may be contributed to by the difficulty of manually controlling the parameters during production, and possibly even the degradation of the filament. Samples investigated directly on the substrate do not display the discrepancy in morphology, as described above. This is most likely due to the fact that the material is un-disturbed, and the last level of particle deposit is investigated on the surface.

Two of the key indicators of quality in nanoparticles are their size and size distribution. Ideally, primary particles will be loose (powder), but generally tend to agglomerate and aggregate, to form larger units or aggregates [4]. An example of an agglomerate is given in Figure 6.9(b), which is an enlargement of Figure 6.9(a).

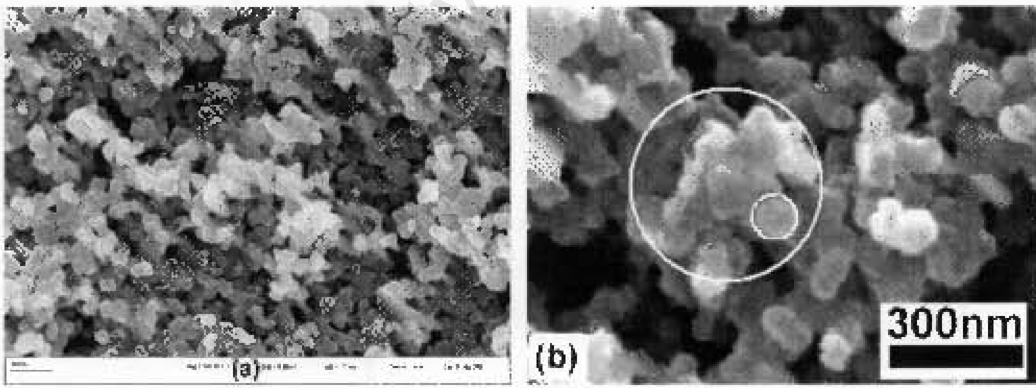

Figure 6.9: (a) Agglomeration of particles to form a porous layer. (b) enlargement of (d), showing formation of aggregates from smaller units

Although the particles in Figure 6.9(a) seem quite separated, the large circle in Figure 6.9(b) shows the diameter of the agglomerate. It is quite larger than a primary particle, indicated by the small circle. As no instrument is available to determine particle size, and size distribution accurately, a method was devised, using the SEM micrographs and

image processing software. To illustrate the process, a SEM of the i-Si mentioned at the beginning of this chapter is used (Figure 6.10(a)). Circular discs are placed on definable particles (Figure 6.10(b)), matching their diameter, using ImageJ 1.36b. The discs serve as a spherical approximation of definable primary particles in the image.

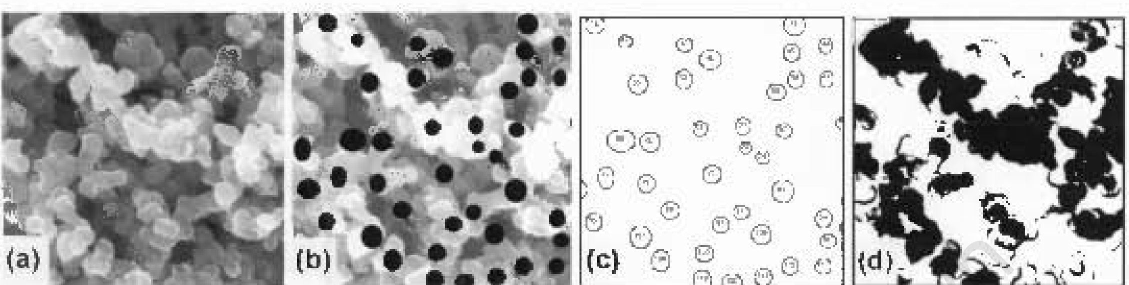

Figure 6.10: Particle size determination using; (a) the original image; (b) placing sized circles; (c) processing the circles; (d) unsuccessful particle filter

After calibration of the image scales, using the SEM scale bar (0.267pixel/nm), a threshold filter is run to remove the background and keep the discs. The "Analyse Particles" module is activated in the diameter measurement mode, which numbers each particle and calculates its diameter and area (Figure 6.10(c)). To calculate the particle size distribution, the "Distribution" module in the software is run, with a binning of 20. Figure 6.11 shows three results of the technique. An attempt was also made to use commercial software (Analysis V 3.1) to determine particle size, but even with manual threshold settings, and thorough experimentation of image parameters, primary particles could not be separated properly (Figure 6.10(d)).

University of Cape Town

Using the technique described above, three sets of images have been processed for particle size, the first two being sample 21 (Figure 6.11(a)) and sample 44 (Figure 6.11(b)), produced at 3 and 24 mbar, and 60 and 40% hydrogen dilution respectively. The third is a sample of the commercial intrinsic silicon (i-Si).

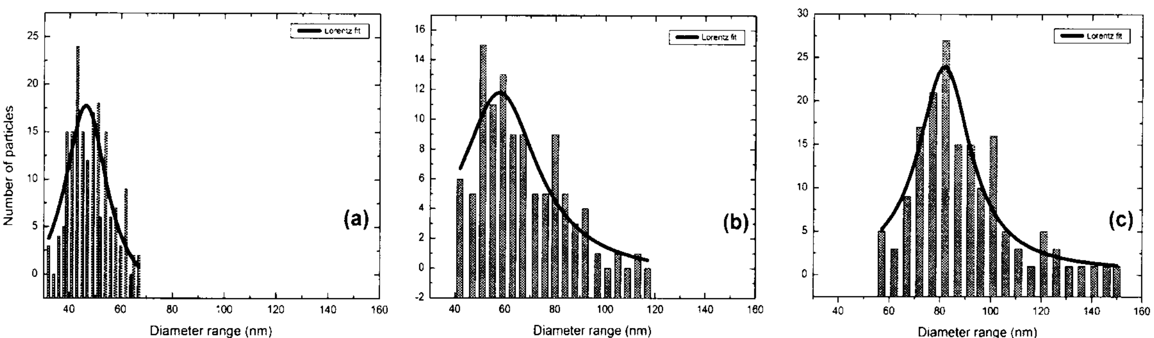

Figure 6.11: Particle size distribution; (a) Sample 21 (b) sample 44 (c) i-Si

Lorentz fits of the data show an average particle diameter of 46.3 nm for sample 21 (Figure 6.11(a)), with a distribution of 20.31 nm, an average diameter of 57.6 nm for sample 24 (Figure 6.11(b)), and 81.6 nm for the i-Si nanoparticles (Figure 6.11(c)). The results indicate that hydrogen dilution may play a role in reducing the primary particle size. Due to the manual and tedious nature of the process, no additional samples have been analysed.

6.3 Particle composition

In the previous section it was shown that nanoparticles have been produced. For particle composition analysis, EDX and FTIR were used, as described in chapter 5. EDX spectra were collected for samples 11, 33, 35, 51 and 55. In preparation for the SEM, all samples were carbon coated, prior to the investigation. As an example, the spectrum, collected for sample 35 is given in Figure 6.12. The sample was produced at 48 mbar and 40% hydrogen dilution.

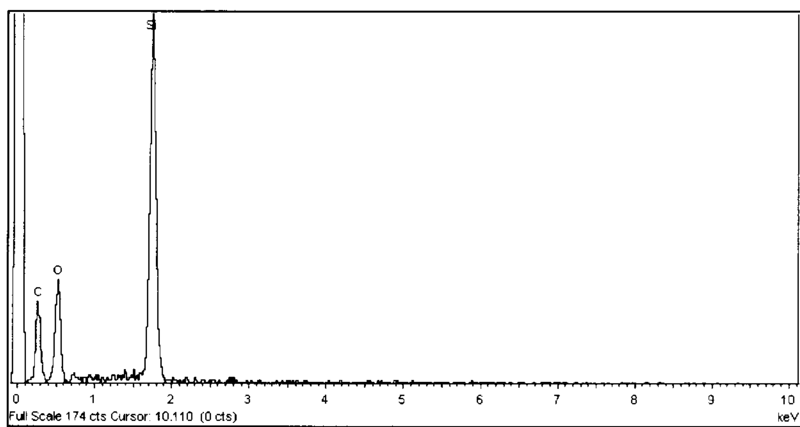

Figure 6.12: EDX spectra of sample 35, produced at 12mbar and 40% H_2

University of Cape Town

As can be seen in the spectrum (Figure 6.12), four major peaks have been registered, of which, the peak at 0 keV is due to an artefact of electronic noise. The presence of carbon can be ascribed to the coating mentioned above, and the remaining two peaks indicate the presence of oxygen and Si. The spectra can be used for a rough estimation of the ratio of these elements present in the particles. Spectra of all samples investigated are similar, in the sense that no unexpected elements have been revealed. The difference between samples is in the atomic ratio of oxygen to silicon of the particles.

These atomic ratios of all samples have been determined by the EDX software and, in Figure 6.13 and Figure 6.14, will be presented as function of pressure and hydrogen dilution.

In Figure 6.13, the atomic ratio of oxygen to that of silicon is given, per sample, at the production pressure. Data points indicate a general slope from the higher to lower pressures, which can be interpreted as a tendency of increased oxygen content in the particles, with a decrease in pressure.

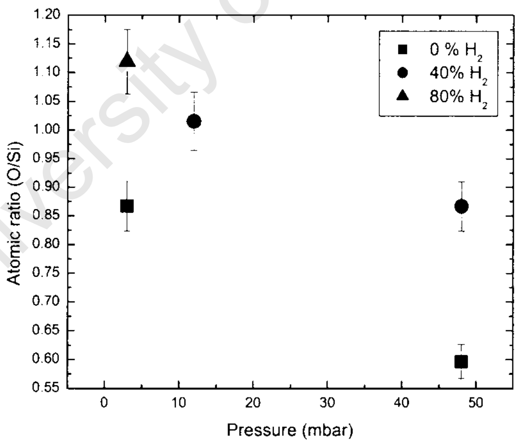

Figure 6.13: Oxygen to silicon atomic ratio as a function of pressure

In Figure 6.14, the data points indicate a positive slope towards higher hydrogen dilutions. This trend can be interpreted as an increase in oxygen content, with an increase in hydrogen dilution.

University of Cape Town

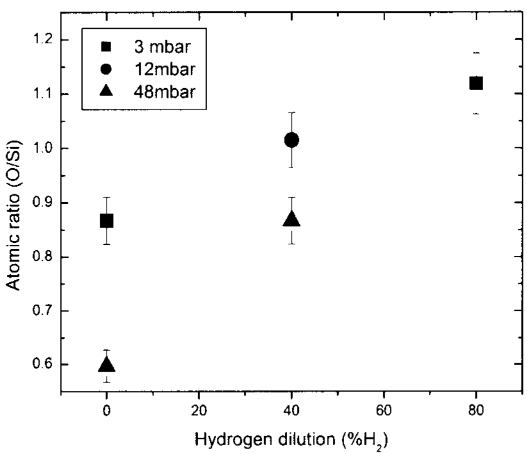

Figure 6.14: Oxygen to silicon atomic ratio as a function of hydrogen dilution

Both of the above mentioned trends are consistent with the presence of residual oxygen in the system, which could be the cause of the high oxygen content found in some of the samples. The effect of the changing pressure and hydrogen content, on the oxygen content present in the material, can be described as follows: An increase in pressure increases the silicon (silane) present in the reactor, thus reducing the oxygen to Si ratio in the gas. Furthermore, an increase in hydrogen decreases the silicon content in the reactor, leading to an increased oxygen ratio. If the presence of the oxygen is, however, ascribed to surface oxidisation, after production, the surface area of the particles (diameter) might be a significant contributor, through the availability of more oxygen binding sites. Atomic ratios for SiO_2 and i-Si were also measured using EDX, and resulted in ratios of 2.03 and 0.19 respectively. The SiO_2, collected at the exhaust output of the production system, shows a near stoichiometric composition.

Further investigations of the composition of the nanoparticles, were performed, using FTIR spectroscopy. Spectra were collected for samples 11, 21, 23, 33, 35 and 51, using the preparation and measurement process described in chapter 5. FTIR spectra can reveal information on the nature of the silicon bonds with hydrogen and oxygen. In silicon thin films these bonds can give an indication of the quality of the material [33]. The absorption peaks, and what they signify, have already been discussed in chapter 5. In Figure 6.15, the major peaks are again shown by means of an infrared spectrum, taken in transmission mode, of a typical nanoparticle sample produced.

University of Cape Town

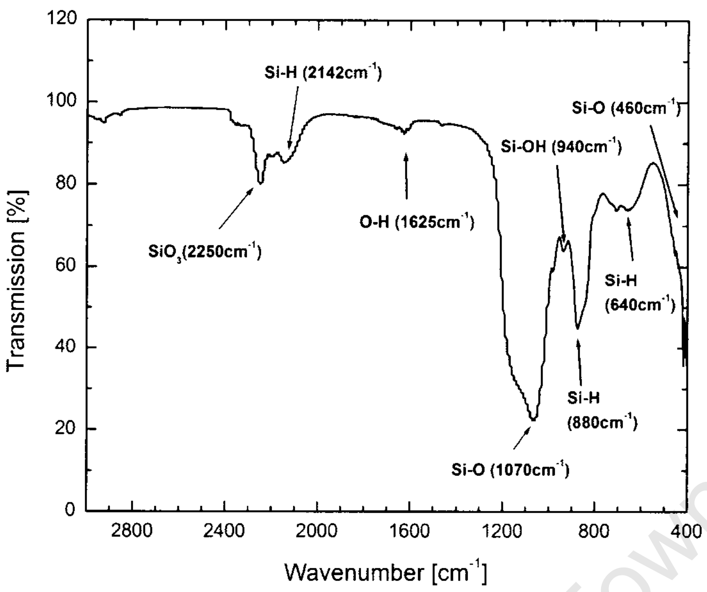

Figure 6.15: Infrared (IR) spectrum in transmission mode, of a typical nanoparticle (powder) sample

Of all the spectra collected, two sets of IR spectra will be discussed. The first set (Figure 6.16), comprises samples 21, 33 and 35, produced at changing operating pressures, and the second set (Figure 6.17), comprising samples 11, 33 and 51, produced at changing hydrogen dilutions.

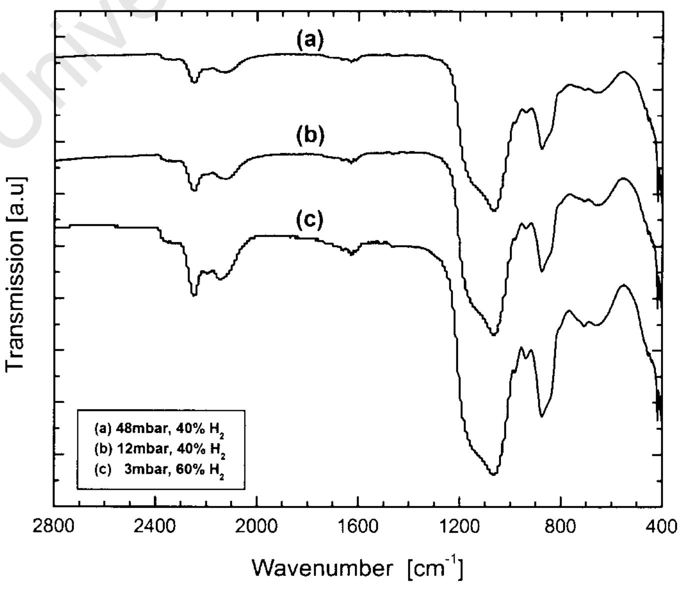

Figure 6.16: Effect of pressure (FTIR spectra)

University of Cape Town

In Figure 6.16, definite and pronounced absorption peaks can be seen at 460, 640, 880, 1070, 2142, and 2250 cm^{-1}. The high absorption by the Si-O bonds at 1070 cm^{-1}, points to oxidisation, and is possibly attributable to the surface oxidisation, which most likely occurred immediately upon exposing the sample to atmosphere [8,33]. It could also point to the presence of residual oxygen in the system. Further evidence of oxidisation lies in the O-H bending vibrations at 1625 cm^{-1}, and the Si-O wagging vibrations at 460 cm^{-1}, as well as Si-O_3 vibrations at 2250 cm^{-1} [31,71]. In the Si nanopowders produced, the absence of a distinctive Si-H absorption peak at about 2000 cm^{-1}, compared to a-Si:H thin films [71] is apparent. Furthermore, in the particles produced, no expected, dominant $(SiH_2)_n$ peak 2100 cm^{-1}, can be observed. Absorption peaks at 640 cm^{-1} and 880cm^{-1} indicate expected surface bound hydrogen in the material. No clear effect of the change in pressure, on the nature of the bonds discussed above, could be found.

In Figure 6.17, the effect of hydrogen dilution on the bonding structure will be discussed.

University of Cape Town

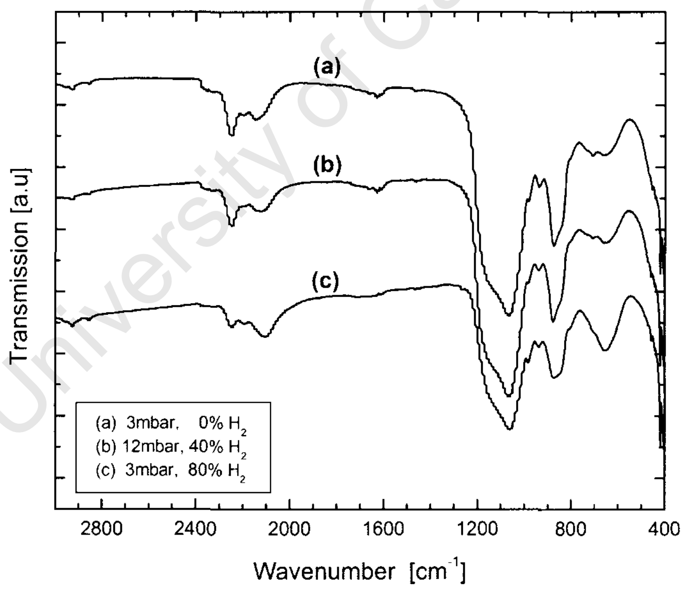

Figure 6.17: Effect of hydrogen dilution (FTIR spectra)

It can be noted, in Figure 6.17, that the ratio between the Si-O peak at 2250 cm^{-1}, and the Si-H peak at 2142 cm^{-1}, changes with a change in hydrogen dilution. These peaks indicate surface bound oxygen and surface bound hydrogen, respectively. When the production conditions exclude hydrogen dilution (Figure 6.17 (a)), the Si-O peak is

dominant, but when the hydrogen dilution is increased to 80% (Figure 6.17 (c)), the Si-H peak is dominant. The latter sample has thus a higher rate of surface bound hydrogen. Figure 6.18 offers a closer look at the ratios as discussed above.

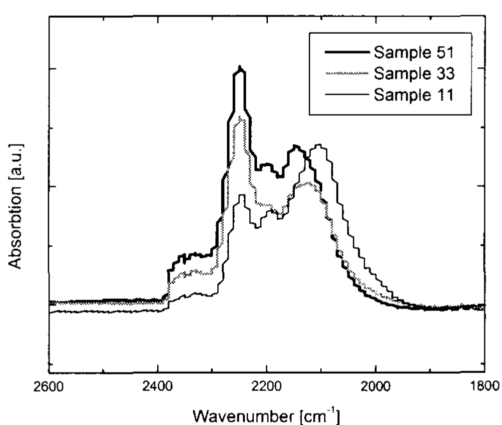

Figure 6.18: A closer look at the 2250 and 2142 cm^{-1} peaks

University of Cape Town

6.4 Crystallinity and crystalline fraction

To get an indication of crystallinity and crystalline fraction of the nanoparticles produced, XRD and RAMAN spectroscopy is performed on a few samples.

XRD was performed on i-Si and on a sample collected from the aperture plate, after production of series 2. This sample was dark brown in colour and was produced at 60% hydrogen dilution, while the pressure was varied. The XRD spectra of these samples are given in Figure 6.19. The spectrum of the benchmark intrinsic nanoparticles (Figure 6.19(a)) displays clear crystalline peaks of silicon [31], at ~28.5°, corresponding to the (111) crystalline orientation, and at ~47° and ~56°, corresponding to the (220) and (311) crystal orientation, respectively. The spectrum of the dark brown particles, produced at temperatures exceeding 120°C (Figure 6.19(b)), has a corresponding broad peak at the (111) reflection and second broad peak between 47° and 56°, with a suggestion of the (220) crystalline peak at 48°. Taken together these observations are indicative of a generally amorphous material with some crystalline order.

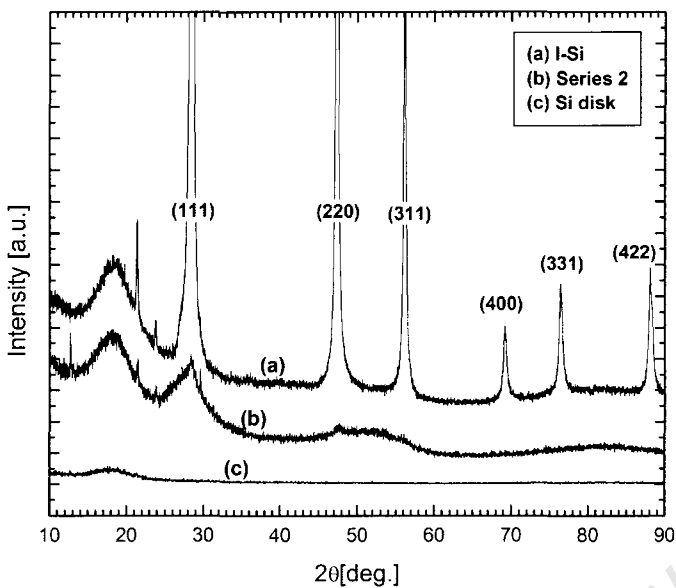

Figure 6.19: XRD spectra of as-deposited material and commercial material

University of Cape Town

The spectrum of the Si support disk and the Vaseline (Figure 6.19(c)) show a possible contribution to the other spectra, from the broad peak at ~18°. It should be noted that the spectrum of the silicon support disk was taken at 1 sec intervals, while the other spectra were taken at 10 sec intervals.

At least 15 samples, produced during the testing of the synthesis system, were taken for Raman spectroscopy, with the purpose of getting to know the technique, and to possibly help with the design of the parameter space. These initial attempts at collecting Raman spectra, using silicon nanoparticles, failed in most samples due to spontaneous exothermic oxidisation of the sample, triggered by the laser energy. Depending on the material, the oxidisation could occur in a fast flash of orange light over the whole sample, or in the form of many tiny bright orange "balls of light", propagating away from the laser and "burning" grooves into the material, and/or resulting in white coloured powder. Either way, the sample was destroyed in the process. An attempt to reduce the laser power by 80% did not stop the oxidisation, and furthermore delivered poor spectra. A second attempt to collect Raman spectra for the samples produced in this research, according to the parameter matrix, again failed. This phenomenon thus prevented a thorough Raman investigation and limits the available spectra to a few

survivors of the earlier investigation. To illustrate the value of the technique, three examples of spectra will be discussed below.

The spectrum given in Figure 6.20 (a) originates from a sample produced at 0.2 mbar, with a flow rate of 40 sccm of silane, at filament and substrate temperatures of 1600 °C and 70 °C respectively. The spectra show a broad peak, centred around 480 cm^{-1}, consistent with amorphous material. Upon accidental spontaneous oxidisation of the sample, as described earlier, a second spectrum (Figure 6.20(b)) was collected from the same sample, resulting in a narrower peak, centred at about 510 cm^{-1}.

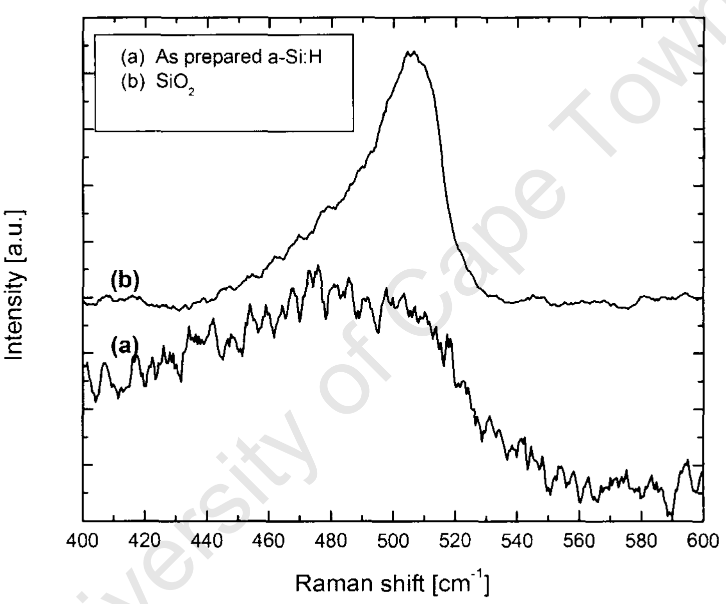

University of Cape Town

Figure 6.20: Raman spectra of (a) a-Si:H (b) SiO_2

Another sample, with a dark brown colour, collected from the wall of the reactor, where the temperature frequently exceeds 120 °C during the experiments (Figure 4.13), was also characterised. The sample was produced at 0.2 mbar, 50 sccm of 90% hydrogen diluted silane, and filament temperature of 1700°C.

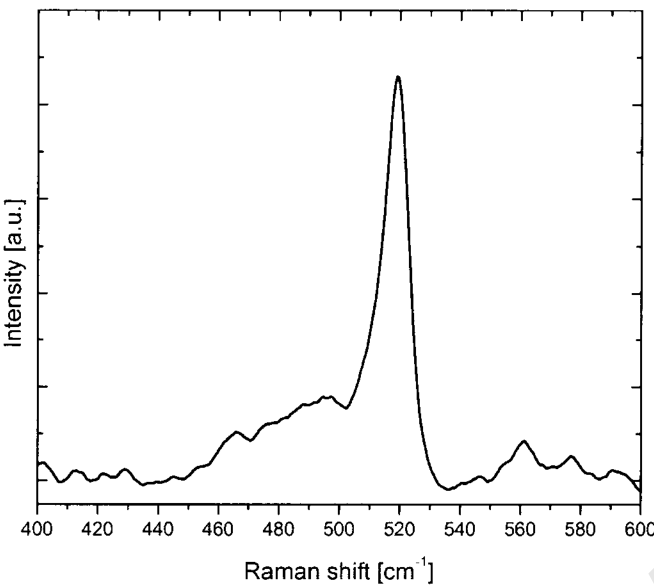

Figure 6.21: Raman spectra of Si:H nanoparticles

The spectrum, given in Figure 6.21 has a broad peak between 460 cm^{-1} and 510 cm^{-1}, indicating the amorphous nature of the material, while the sharper peak at 520 cm^{-1} signifies a crystalline contribution [59]. As a first approach, and not taking into account a possible dependency on the average crystallite size, the crystalline volume fraction of the sample was calculated [80], to be 0.52, using the equation:

$$V_f = \frac{I_{520}}{I_{520} + I_{480}} \qquad (6.1)$$

where, I_{520} and I_{480} are the areas of the peaks at about 520 cm^{-1} and 480 cm^{-1} of the de-convoluted Raman spectrum. This result may indicate that particles collected on a surface of higher temperature have an increase of order in the structure of the particles.

University of Cape Town

7. CONCLUSION

The hypotheses that thermal catalytic pyrolysis (HWCVD) is a viable method for the production of silicon nanoparticles has been proven to be true. Silicon nanopowders deposit on all surfaces in the reactor, and are yellowish to dark brown in colour. Amorphous silicon nanoparticles, in the 40 to 100 nm size range, are produced under most conditions tested. While material with a crystalline contribution has been found, the operating parameters that control particle size and crystallinity could not be clearly identified.

Most material produced consists of highly porous deposits of agglomerated, and in some cases aggregated, amorphous nanoparticles. Particles produced at the experimental conditions of substrate temperatures below 70 °C were always yellowish to brown in colour and amorphous, while some dark brown materials, which were collected near the filament, where the temperature exceeds 120 °C, showed a crystalline contribution. This can be interpreted as an indication, that the high substrate temperatures play an important part in ordered growth, even for nanoparticle deposition. FTIR spectra of the particles reveal high concentrations of hydrogen, presumed to passivate silicon dangling bonds. The presence of absorption peaks, indicating substantial surface oxidisation, can be linked to either post production removal of the samples from the vacuum and subsequent exposure to atmosphere, or incorporation of residual oxygen in the reactor during deposition.

University of Cape Town

As expected, the production rate of material produced at the same pressure, filament temperature and flow rate, increases linearly with decrease in hydrogen dilution. This can simply be ascribed to the decrease of the precursor, silane. Furthermore, an increase in pressure was expected to lead to increased interaction of species in the vapour phase, and thus to a higher production rates. The opposite has been observed. In general, the production rate decreases with an increase in pressure. This decrease is partly due to an accelerated deterioration of the filament in relatively high pressure regimes.

As far as the control of filament temperature is concerned, only a single colour pyrometer has been available for the experiments, which was found difficult to use for wire temperature measurements, especially where the emissivity changes over time. As two colour pyrometer measurements are not reliant on emissivity, such instrument will be more advisable for future experiments. For further study of thermal catalytic pyrolysis of silicon nanoparticles it is also highly recommended to improve the pumping capacity of the vacuum pump, and improve the sensitivity of the mass flow controllers. These improvements will not only permit experiments at lower pressure regimes, where the filament is expected to deteriorate at a lower rate, but will also reduce the basic pressure of the system, thus reducing potential contamination with residual air. The lower pressure regime will furthermore allow further investigation into the parameters that will lead to controlled particle size and crystalline fraction.

University of Cape Town

REFERENCES

[1] K.-H. Haas and F. Hutter. Produktion von und mit nanomaterialien. Untersuchen des Forschungs-und Handlungsbedarfs für die industrielle Produktion. Fraunhofer-Institut für Silicatforschung, Schlussbericht (2003).

[2] H. Gleiter. Nanostructured materials: basic concepts and microstructure. Acta Materialia, 48 (2000) 1.

[3] A. Sasaki. Size distribution analysis of nanoparticles using small angle x-ray scattering technique. The Rigaku Journal, 22 no. 1 (2005) 31.

[4] A. Gutsch, M. Krämer, G. Michael, H. Mühlenweg, M. Pridöhl and G. Zimmermann. Degussa AG, Gas-Phase Production of Nanoparticles. KONA, 20 (2002).

[5] F. E. Kruis, H. Fissan and A. Peled. Synthesis of nanoparticles in the gas phase for electronic, optical and magnetic applications - a review. J. Aerosol Sci., 29 (1998) 511.

[6] A. Babat, C. Anderson, C. R. Perry, C. B. Carter, S. A. Campbell and U. Kortshagen. Plasma synthesis of single-crystal silicon nanoparticles for novel electronic device applications. Plasma Phys. Control. Fusion, 46 (2004) B97-B109.

[7] D. T. Britton and M. Härting. Printed Nanoparticulate Composites for Silicon Thick Film Electronics. Pure Appl. Chem., 78 (2006) 1723.

[8] M. L. Ostraat, M. Brongersma, H. A. Atwater and R. C. Flagan. Nanoengineered silicon dioxide nanoparticle heterostructures. Solid State Sci. , 7 (2005) 882.

[9] G. Singhal, A. Wang, N. Glumac, B. H. Kear and R. D. Hunt. On nanoparticle aggregation during vapor phase synthesis. NanoStructured Materials, 11 No. 4 (1999) 545.

[10] *Oxford Dictionary of Chemistry*, Oxford University Press.

[11] R. J. Aitken, K. S. Creely and C. L. Tran, "Nanoparticles: An occupational hygiene review," Report No. ISBN 0 7176 2908 2 (2004).

[12] D. T. Britton and M. Härting. Printed Nanoparticulate Composites for Silicon Thick Film Electronics. Conference: WAM II, (2005).

[13] C. Lam, Y. F. Zhang, Y. H. Tang, C. S. Lee, I. Bello and S. T. Lee. Large-scale synthesis of ultra fine Si nanoparticles by ball milling. Journal of Crystal Growth, 220 (2000) 466.

[14] C. Araujo-Andrade, F. J. Espinoza-Beltran, S. Jimenez-Sandoval and J. Gonzalez-Hern. Synthesis of nanocrystalline Si particles from a solid-state reaction during a ball-milling process. Scripta Materialia, 49 (2003) 773.

University of Cape Town

[15] M. T. Swihart. Vapor-phase synthesis of nanoparticles. Current Opinion in Colloid and Interface Science, 8 (2003) 127.

[16] M. H. Wu, R. Mu, A. Ueda and D. O. Henderson. Micro Raman Spectroscopy of Silicon Nano-crystals produced by Pico-second Pulsed Laser Ablation. Material Research Society Symposium Proceedings, 738 (2003).

[17] M. H. Nayfeh, J. Therrien and Z. H. Mani, World Intellectual Property Organisation ed. (United States Patent Application, 2001).

[18] Y. Leconte, P. Marie, X. Portier, M. Lejeune and R. Rizk. Combined growth of Si nanoparticles and crystallized silicon layers at 200deg C by reactive magnetron sputtering. Materials Science and Engineering, B101 (2003) 194.

[19] Y. Zhu, H. Wang and P. P. Ong. Preparation and thermal stability of silicon nanoparticles. Applied Surface Science, 171 (2001) 44.

[20] C. Chazelas, J. F. Coudert, J. Jarrige and P. Fauchais. Synthesis of ultra fine particles by plasma transferred arc: Influence of anode material on particle properties. Journal of the European Ceramic Society, (2006).

[21] L. Mädler. Liquid-fed Aerosol Reactors for One-step Synthesis of Nano-structured Particles. KONA, 22 (2004).

[22] Q. Liu and S. M. Kauzlarich. A new synthetic route for the synthesis of hydrogen terminated silicon nanoparticles. Materials Science and Engineering, 96 (2002) 72.

[23] S. M. Kauzlarich, Q. Liu, S.-C. Yin and H. W. H. Lee. The Novel Synthesis of Silicon and Germanium Nanocrystallites. Mat. Res. Soc. Symp. Proc., 638 (2001).

[24] B. D. Rowsell and J. G. C. Veinot, *Reductive thermolysis of heterocyclic precursors: a convenient method for preparing luminescent, surfactant-stabilized silicon nanoparticles*, 2005).

[25] K. Nakaso, B. Han, K. H. Ahn, M. Choi and K. Okuyama. Synthesis of non-agglomerated nanoparticles by an electrospray assisted chemical vapour deposition (ES-CVD) method. Aerosol Science, 34 (2003) 869.

[26] K. Wegner, W. J. Stark and S. E. Pratsinis. Flame-nozzle synthesis of nanoparticles with closely controlled size, morphology and crystallinity. Materials Letters, 55 (2002) 318.

[27] G. Ledoux, D. Amans, J. Gong, F. Huisken, F. Cichos and J. Martin. Nanostructured films composed of silicon nanocrystals. Materials Science and Engineering, 19 (2002) 215.

University of Cape Town

[28] R. Giorgi, S. Turth, G. Zappa, E. Borsella, S. Botti, M. C. Cesile and S. Martelli. Microstructural properties of laser synthesized Si/C/N nanoparticles. Applied Surface Science, 93 (1996) 101.

[29] F. Huisken, H. Hofmeister, B. Kohn, M. A. Languna and V. Paillard. Laser production and deposition of light-emitting silicon nanoparticles. Applied Surface Sciences, 154 (2000) 305.

[30] J. J. Najera, J. O. Caceres, J. C. Ferrero and S. I. Lane. Production of silicon containing particles by laser induced reaction of silane with methane, ethane and acetylene. Journal of the European Ceramic Society, 22 (2002) 2371.

[31] J. Knipping, H. Wiggers, B. Rellinghaus, P. Roth, D. Konjhodzic and C. Meier. Synthesis of High Purity Silicon Nanoparticles in a Low Pressure Microwave Reactor. J. Nanosci. Nanotechnol. , 4 (2004) 1039.

[32] C. Meier, S. Luttjohanna, V. G. Kravetsa, A. Nienhaus, H. Lorkea, H. Wiggers, C.-K. Choo, T. Sakamoto, M. Tohara, K. Tanaka, R. Nakata and N. Okuyama. Raman properties of silicon nanoparticles preparation and evaluation of nitrogen-terminated silicon nanoparticles: laser annealing effect. Physica E, 32 (2006) 155.

[33] R. E. I. Schropp, B. Stannowski, A. M. Brockhoff, P. A. T. T. Van Veenendaal and J. B. Rath. Hot wire CVD heterogeneous and polychrystalline silicon semiconductor thin films for applications in thin film transistors and solar cells. Mater.Phys.Mech, (2000) 73.

[34] Q. Wang. Combinatorial approach to studying tungsten filament ageing in fabricating hydrogenated amorphous silicon using the hot-wire chemical vapour deposition technique. Meas. Sci. Technol., 16 (2005) 162.

[35] N. M. Hwang, W. S. Cheong, D. Y. Yoon and D.-Y. Kim. Growth of silicon nanowires by chemical vapor deposition: approach by charged cluster model. Journal of Crystal Growth, 218 (2000) 33.

[36] A. H. Mahan. An update on silicon deposition performed by hot wire CVD. Thin Solid Films, 501 (2006) 3.

[37] H. Matsubara and T. Sakuma. Diamond deposition on cemented carbide by chemical vapour deposition using a tantalum filament. Journal of Materials Science, 25 (1990) 4472.

[38] K. K. S. Lau, Y. Mao, H. G. Pryce Lewis, S. K. Murthy, B. D. Olsen, L. S. Loo and K. K. Gleason. Polymeric nanocoatings by hot-wire chemical vapor deposition (HWCVD). Thin Solid Films, 501 (2006) 211-215.

University of Cape Town

[39] H. Wiesmann, A. K. Gosh, T. McMahon and M. Strongin. Journal of Applied Physics, 50 (1979) 3752.

[40] M. Matsumura and M. Tachibana. Applied Physics Letters, 47 (1985) 833.

[41] M. Matsumura. Japan Journal of Applied Physics, 25 (1986) 949.

[42] J. Doyle, R. Robertson, G. H. Lin, M. Z. He and A. Gallagher. Journal of Applied Physics. 64 (1988) 3215.

[43] A. H. Mahan, J. Carapella, B. P. Nelson, R. S. Crandall and I. Balberg. Journal of Applied Physics, 69 (1991) 6728.

[44] Y. Kajikawa and S. Noda. Growth mode during initial stage of chemical vapor deposition. Applied Surface Science, 245 (2005) 281.

[45] K. F. Feenstra, Thesis, Hot-wire chemical vapour deposition of amorphous silicon and the application in solar cells, 1998.

[46] D. M. Kremer, R. W. Davisb, E. F. Mooreb and S. H. Ehrman. A numerical investigation of the effects of gas-phase particle formation on silicon film deposition from silane. Journal of Crystal Growth, 247 (2003) 333.

[47] D. Peiro´, J. Bertomeu, C. Voz, M. Fonrodona, D. Soler and J. Andreu. Structure of microcrystalline silicon films deposited at very low temperatures by hot-wire CVD. Materials Science and Engineering, B69–70 (2000) 536.

[48] M. Zhao. Hot-Wire Chemical Vapor Deposition - an effective way to prepare a-Si & poly-Si. Term paper, ENSC 895.

[49] D. Soler, Thesis, Amourphous silicon solar cells obtained by hot-wire chemical vapour deposition, 2004.

[50] C. E. Richardson, M. S. Mason, H. A. Atwater and T. J. Watson. A Phase Diagram for Morphology and Properties of Low Temperature Deposited Polycrystalline Silicon Grown by Hot-wire Chemical Vapour Deposition. Laboratory of Applied Physics.

[51] K. Brühne, M. B. Schubert, C. Kohler and J. H. Werner. Nanocrystalline silicon from hot-wire deposition - a photovoltaic material? Thin Solid Films, 395 (2001) 163.

[52] D. Soler, M. Fonrodona, C. Voz, J. Bertomeu and J. Andreu. Thin silicon films ranging from amorphous to nanocrystalline obtained by hot-wire CVD. Thin Solid Films, 383 (2001) 189.

[53] S. S. Talukdar and M. T. Swihart. Aerosol dynamics modeling of silicon nanoparticle formation during silane pyrolysis: a comparison of three solution methods. J. Aerosol Sci. , 35 (2004) 889.

University of Cape Town

[54] N. M. Hwang, W. S. Cheong and D. Y. Yoon. Deposition behavior of Si on insulating and conducting substrates in the CVD process: approach by charged cluster model. Journal of Crystal Growth, 206 (1999) 177.

[55] N. M. Hwang, J. H. Hahn and D. Y. Yoon. Charged Cluster Model in HWCVD. J. Cryst. Growth, 162 (1996) 55.

[56] N.-M. Hwang and D.-Y. Kim. Charged clusters in thin film growth. International Materials Reviews, 49 (2004).

[57] W. S. Cheong, N. M. Hwang and D. Y. Yoon. Observation of nanometer silicon clusters in the hot-filament CVD process. Journal of Crystal Growth, 204 (1999) 52.

[58] I. Ferreira, A. Cabrita, F. F. Braz, E. Fortunato and R. Martins. Role of the gas pressure and hydrogen dilution on the properties of large area nanocrystalline p-type silicon films produced by hot wire technique. Materials Science and Engineering, 15 (2001) 141.

[59] S. Nakamura and M. Koshi. Elementary processes in silicon hot wire CVD. Thin Solid Films, 501 (2006) 26.

[60] H. S. Povolny and X. Deng. High-rate deposition of amorphous silicon films using hot-wire CVD with a coil-shaped filament. Thin Solid Films, 430 (2003) 125.

[61] W. S. Cheong, D. Y. Yoon, D.-Y. Kim and N. M. Hwang. Effect of substrates on morphological evolution of a film in the silicon CVD process: approach by charged cluster model. Journal of Crystal Growth, 218 (2000) 27.

[62] Air-Liquide, in *MSDS Nr: 107 AL*; *Vol. Version: 1.01* (2002).

[63] Scott Specialty Gases: Design and Safety. www.scottgas.com, (2004).

[64] X. Deng and H. S. Povolny. Hot-wire deposition of amorphous and microcrystalline silicon using different gas excitations by a coiled filament. Thin Solid Films, 430 (2003) 304.

[65] Goodfellow. Tungsten product specification. www.goodfellow.com, (2006).

[66] D. C. Giancoli, *Physics, Principles with Applications*, Published by Pearson Education Inc.).

[67] in *Viton O-Ring specification. www.mdvacuum.com.* , (2006).

[68] H. A. Atwater. Low-Temperature, High-Throughput Process for Thin, Large-Grained Poly Si. Final Technical Report, NREL/SR-520-34816 (2003).

[69] R. C. Weast, *CRC Handbook of Chemistry and Physics*, CRC Press, Boca Raton, (1979).

[70] R. Martins, I. Ferreira, B. Fernandes and E. Fortunato. Performances of a-Si:H films produced by hot wire plasma assisted technique. Vacuum, 52 (1999) 203.

University of Cape Town

[71] J. Dutta, H. Hofmann, C. Hollenstein and H. Hofmeister. Plasma-Produced Silicon Nanoparticle Growth and Crystallization Processes. Nanoparticles in solids and solutions: preparation, characterization and utilization. Chapter 8 (1998) 173.

[72] N. B. Colthup, L. H. Daly and S. E. Wiberley, *Introduction to Infrared and Raman Spectroscopy*, Atlantic Publishers).

[73] B. Stannowski, C. H. M. van der Werf and R. E. I. Schroop. Hot-wire chemical-vapour deposition for low-temperature deposition of silicon-nitride layers. Proc. of the 3rd Intern. Conf. on Coatings on Glass, (2000) 387.

[74] ICDD. International Centre for Diffraction Data. www.icdd.com, (2006).

[75] C. Kittel, *Introduction to Solid State Physics*, John Wiley & Sons, Inc., 2005).

[76] D. T. Britton, A. Hempel, M. Härting, G. Kögel, P. Sperr, W. Triftshäuser, C. Arendse and D. Knoesen. Annealing and recrystallisation of hydrogenated amorphous silicon. Phys. Rev. B: Condens. Matter Mater. Phys., B64 (2001).

[77] E. Bustarret, M. A. Hachicha and M. Brunel. Experimental determination of the nanocrystalline volume fraction in silicon thin firms from Raman spectroscopy. Applied Physics Letters, 52 (1988) 1675.

[78] N. Chaabane, P. Roca i Cabarrocas and H. Vach. Trapping of plasma produced nanocrystalline Si particles on a low temperature substrate. Journal of Non-Crystalline Solids, 338-340 (2004) 51-55.

[79] in *MTI Corporation. Nanopowder specifications.* *http://www.mticrystal.com*, (2006).

[80] I. Ferreira, A. Cabrita, F. F. Braz, E. Fortunato and R. Martins. Morphology and structure of nanocrystalline p-doped silicon films produced by hot wire technique. Vacuum, 64 (2002) 237.

University of Cape Town

APPENDIX "A": Gas handling safety control-sheet

Gas handling Safety control-sheet

M Scriba 7/2/2006

(D:\Silicon\Safety\Gas Handling Safety control sheet.doc)

	Safety Valves (Roof)		Gas Lines			
Date/Time	**Cylinder**	**S1**		**Green**	**Blue**	**Chamber**
2006/2/2 10:15	Open	Open	10 µBar, N_2	10 µBar, N_2	10 µBar, N_2	10 µBar, N_2
12:10	Open	Open	2 Bar Silane	2 Bar Silane	10 µBar, N_2	Air
15:10	Close	Close	2 Bar N_2	2 Bar N_2	2 Bar N_2	Air

University of Cape Town

APPENDX "B": Gas safety posters

SiH_4	**Silane** Monosilane, Silicane Silicon Hydride Silicon Tetrahydride	Based on MSDS Nr. 107_AL (Air Liquide Version 1.01)
Physical properties	Colour	Colourless
	Physical Form	Gas
	Odour	Unpleasant Odour
Hazards Identification	**Extremely Flammable.** Spontaneous ignition in contact with air.	
First Aid Measures	**In high concentration** may cause asphyxiation May cause headache, nausea and irritation of respiratory tract Symptoms may include loss of mobility/consciousness. Victim may not be aware of asphyxiation	Remove person from area wearing self contained breathing apparatus **Apply artificial respiration**
	Burning	Treat like normal burn.
Fire Fighting Measures	**Escaping gas can not be extinguished**	
	Suitable Extinguishing media	Water Carbon Dioxide All known extinguishers can be used
	Unsuitable extinguishing media	Halons
	Method **Location of STOP VALVE** Below window towards the gas cylinder. Marked Silane STOP VALVE	Stop gas flow ASAP – STOP VALVE Move away from the container and cool with water from protected position. Do not extinguish a leaking gas flame unless absolutely necessary Spontaneous/explosive re-ignition may occur Extinguish any other fire. Cylinder on roof of building 14D **Keys below**
Accidental Release Measures	Personal precautions	Wear self–contained breathing apparatus when entering area Evacuate area Ensure adequate air ventilation Eliminate ignition sources.
	Environmental precautions	Stop release ASAP Prevent from entering lower areas basements etc.
	Clean up methods	Ventilate area Vacuum clean the area
Stability and Reactivity	Stability and Reactivity	Can form explosive mixtures with air Ignites spontaneously with air May react violently with oxidants
Toxicology Information	General	May cause nausea and irritation of the respiratory tract. Hydrolysis in the body form silicic acid or hydrated silica.

DANGER
CHEMICAL SPILL

Contact: Manfred Scriba
Room: F119, 082 457 0657
CSIR: x2222

University of Cape Town

H_2	Hydrogen	Based on MSDS Nr: 067A_AL (Air Liquide Version 1.01)
Physical properties	Colour	Colourless
	Physical Form	Gas
	Odour	Odourless
Hazards Identification	Extremely Flammable.	
First Aid Measures	In **high concentration** may cause asphyxiation. Symptoms may include loss of mobility/consciousness. Victim may not be aware of asphyxiation.	Remove person from area wearing self contained breathing apparatus. Apply artificial respiration.
	Burning	Treat like normal burn.
Fire Fighting Measures	Suitable Extinguishing media	All known extinguishers can be used.
	Method Location of H2 Cylinder: Gas storage between Building 14F and 14E. Cubicle marked H2. Keyes below	Stop gas flow ASAP. Move away from the container and cool with water from protected position. Do not extinguish a leaking gas flame unless absolutely necessary. Spontaneous/explosive re-ignition may occur. Extinguish any other fire.
Accidental Release Measures	Personal precautions	Wear self-contained breathing apparatus when entering area. Evacuate area. Ensure adequate air ventilation. Eliminate ignition sources.
	Environmental precautions	Stop release ASAP. Prevent from entering lower areas, basements etc.
	Clean up methods	Ventilate area.
Stability and Reactivity	Stability and Reactivity	Can form explosive mixtures with air. May react violently with oxidants.
Toxicology Information	General	No toxicological effects from this product

Contact: Dr Chris Arendse
Room: F143, 0844036043

CSIR: x2222

University of Cape Town